Cytosine and adenine base editing of the brain, liver, retina, heart and skeletal muscle of mice via adeno-associated viruses

Jonathan M. Levy[1,2,3], **Wei-Hsi Yeh**[1,2,3,4], **Nachiket Pendse**[5,6], **Jessie R. Davis**[1,2,3], **Erin Hennessey**[5,6], **Rossano Butcher**[5,6], **Luke W. Koblan**[1,2,3], **Jason Comander**[5,6], **Qin Liu**[5,6], **David R. Liu**[1,2,3,*]

[1]Merkin Institute of Transformative Technologies in Healthcare, Broad Institute of Harvard and MIT, Cambridge, MA, USA

[2]Department of Chemistry and Chemical Biology, Harvard University, Cambridge, MA, USA

[3]Howard Hughes Medical Institute, Harvard University, Cambridge, MA, USA

[4]Program in Speech and Hearing Bioscience and Technology, Harvard Medical School, Boston, MA, 02115, USA.

[5]Ocular Genomics Institute, Massachusetts Eye and Ear Institute, Boston, MA, USA

[6]Department of Ophthalmology, Harvard Medical School, Boston, MA, USA

Abstract

The success of base editors for the study and treatment of genetic diseases depends on the ability to deliver them in vivo to the relevant cell types. Delivery via adeno-associated viruses (AAVs) is limited by AAV-packaging capacity, which precludes the use of full-length base editors. Here, we report the application of dual AAVs for the delivery of split cytosine and adenine base editors that are then reconstituted by trans-splicing inteins. Optimized dual AAVs enable in vivo base editing at therapeutically relevant efficiencies and dosages in the mouse brain (up to 59% of unsorted cortical tissue), liver (38%), retina (38%), heart (20%) and skeletal muscle (9%). We also show that base editing corrects, in mouse brain tissue, a mutation that causes Niemann-Pick disease type C (a neurodegenerative ataxia), slowing down neurodegeneration and increasing the animals'

*Correspondence should be addressed to David R. Liu: drliu@fas.harvard.edu.

lifespan. The optimized delivery vectors should facilitate the efficient introduction of targeted point mutations into multiple tissues of therapeutic interest.

Point mutations represent the majority of known pathogenic human genetic variants[1]. To enable the direct installation or correction of point mutations in living cells, we developed base editors, engineered proteins that directly convert a target base pair to a different base pair without creating double-stranded DNA breaks[2–4]. Cytosine base editors (CBEs) such as BE4max[3,5–7] catalyze the conversion of target C•G base pairs to T•A, while adenine base editors (ABEs) such as ABEmax[4,6] convert target A•T base pairs to G•C. While CBEs and ABEs are both widely used and work robustly in many cultured mammalian cell systems[2], the efficient delivery of base editors into live animals remains a challenge, despite promising initial studies[8–10]. A major impediment to the delivery of base editors in animals has been an inability to package base editors in adeno-associated virus (AAV), an efficient and widely used delivery agent that remains the only FDA- approved *in vivo* gene therapy vector[11]. The large size of the DNA encoding base editors (5.2 kb for base editors containing *S. pyogenes* Cas9, not including any guide RNA or regulatory sequences) precludes packaging in AAV, which has a genome packaging size limit of   5 kb[12,13].

To bypass this packaging size limit and deliver base editors using AAVs, we devised a split-base editor dual AAV strategy[14,15] in which the CBE or ABE is divided into an N-terminal and C-terminal half. Each base editor half is fused to half of a fast-splicing split-intein. Following co-infection by AAV particles expressing each base editor–split intein half, protein splicing in *trans* reconstitutes full-length base editor. Unlike other approaches utilizing small molecules[16] or sgRNA[17] to bridge split Cas9, intein splicing removes all exogenous sequences and regenerates a native peptide bond at the split site, resulting in a single reconstituted protein identical in sequence to the unmodified base editor.

In this study we developed split-intein CBEs and split-intein ABEs, and integrated them into optimized dual AAV genomes that enable the most efficient base editing to date in somatic tissues of therapeutic relevance, including liver, heart, muscle, retina, and brain. We used the resulting AAVs to achieve base editing efficiencies at test loci for both CBEs and ABEs that, in each of these tissues, meets or exceeds therapeutically relevant editing thresholds for the treatment of some human genetic diseases at AAV dosages that are known to be well-tolerated in humans. Integrating these developments, we used dual AAV split-intein base editors to treat a mouse model of Niemann-Pick disease type C, a debilitating disease that affects the central nervous system (CNS), resulting in correction of the casual mutation in CNS tissue, preservation of target neurons, and an increase in animal lifespan.

Results

Development of a split-intein approach to CBE and ABE reconstitution

We reasoned that the use of a *trans*-splicing intein would enable CBE and ABE to be divided into halves that are each smaller than the AAV packaging size limit, enabling dual AAV packaging of base editors (Fig. 1a). To generate a split-intein CBE, we first fused each split DnaE intein half from *Nostoc punctiforme* (Npu)[18] to each half of the original CBE BE3[3], a

fusion protein of rat APOBEC1, *S. pyogenes* Cas9, and uracil glycosylase inhibitor (UGI) from bacteriophage PBS1, dividing BE3 within the *S. pyogenes* Cas9 domain[15,19] immediately before Cys 574 or Thr 638. We observed that dividing BE3 just before Cys 574 with the split Npu intein (referred to hereafter as the Npu-BE3 construct), resulted in robust on-target base editing (34±6.4% average editing by high-throughput sequencing among unsorted cells targeting six genomic loci, Fig. 1b) in HEK293T cells following co-transfection of plasmids expressing each split half, plus a third plasmid expressing sgRNA. Notably, target C•G-to-T•A editing efficiency was higher, rather than lower, than editing levels following transfection of a plasmid expressing an intact BE3, which resulted in an average of 22±7.9% editing across the six sites (Fig. 1b and 1c), indicating that intein splicing at Cys 574 does not limit editing efficiency in this system. We speculate that higher expression levels of each split-intein base editor half, relative to that of the much larger intact base editor proteins, may account for increased editing from split-intein base editors. Interestingly, the second tested BE3 split site, ahead of Thr 638, did not support robust base editing (averaging 10±10% editing across six sites) even though both split sites support Cas9 nuclease activity[15], suggesting that base editors impose additional requirements for productive intein splicing or productive editing compared to Cas9 nuclease.

After identifying a BE3 split site that does not impair base editing efficiency following intein splicing, we next optimized split-intein CBE performance. We compared the performance of the Npu split intein with that of Cfa, a synthetic split intein developed from the consensus sequences of fast-splicing DnaE homologs from a variety of organisms[20]. Npu-BE3 outperformed Cfa-BE3, which resulted in 25±10% average base editing (Fig. 1b and 1c). To incorporate recent architectural improvements in our newer BE4 base editor[5], as well as improved expression and nuclear localization of BE4max[6], we generated Npu-BE4 constructs and tested two codon usages. Consistent with our recent report[6], we observed that codon and nuclear localization signal (NLS) optimization of Npu-BE4max resulted in higher base editing efficiencies than Npu-BE4 using IDT codon optimization (44±4.2% editing vs. 26±3.0% editing, Fig. 1d). We also found that the second uracil glycosylase inhibitor domain, which improves C•G -to-T•A editing outcomes in some architectures[5], did not increase the editing efficiency of Npu-BE4max; a single UGI in the BEmax architecture yields 48±3.0% editing (Fig. 1d and 1e). In light of these results, we omitted the second UGI from future AAV constructs to minimize viral genome size, resulting in a spliced NLS- and codon-optimized APOBEC–Cas9 nickase–UGI construct that we refer to hereafter as CBE3.9max.

We were intrigued by the comparable editing efficiencies of full-length and intein-split base editors. To measure relative expression levels, we performed Western blots in HEK cells transfected with HA- and FLAG-tagged split-halves and an sgRNA targeting the HEK3 locus, finding that the co-expression of the split-halves generates unspliced and full-length CBE3.9max (Supplementary Fig. 1d). Sequencing data show that all constructs efficiently edit the HEK3 locus (Supplementary Fig. 1e). We additionally tested an inactivating split-intein mutation, Npu C1A, that inhibits splicing following intein association[21]. Although these C1A constructs did not generate full-length CBE3.9max, they robustly edited HEK3 (Supplementary Fig. 1d – 1f). These data indicate that in addition to mediating covalent

splicing and reconstitution of full-length base editors, the inteins are able to mediate association of the editor split-halves and generate functional base editor without splicing.

We also used the Cys 574 Cas9 split site and the Npu split intein to generate a split optimized adenine base editor (Npu-ABEmax) construct. To test whether Npu-ABEmax reconstitutes ABEmax[6] activity, we installed a silent mutation in the mouse *DNMT1* locus, which has been shown to be amenable to Cas9 cutting activity[22], in 3T3 cells, finding that Npu-ABEmax and ABEmax have equal activity (63±5.4% A•T-to-G•C editing from Npu-ABEmax, compared to 63±6.3% editing from non-split ABEmax, Fig. 1f). Finally, we screened seven split sites in *S. aureus* Cas9–BE3 (SaBE3)[23], and identified a site immediately before Cys 535 that fully recapitulated unsplit SaBE3 activity in HEK293T cells (Supplementary Fig. 1). A recent report demonstrated that another intein split site, preceding Ser 740, reconstitutes full-length SaCas9 nuclease activity and supports split Sa-BE3 activity *in vivo*[24]. Together, these results establish optimized split-intein CBE and ABE halves that, upon protein splicing, reconstitute cytosine and adenine base editors with no apparent loss in editing efficiency.

Development of split-intein CBE and ABE AAV

After developing a viable way to divide both classes of base editors into split intein-fused halves, we generated and characterized a series of AAV particles to optimize base editing efficiency and minimize AAV genome size to support efficient AAV production[25]. We tested several post-transcriptional regulatory element sequences (PREs) and sgRNA positions in the context of AAV, rather than plasmid delivery, to maximize the *in vivo* relevance of the optimization process.

To avoid effects specific to cultured cells, we used PHP.B[26], an evolved AAV variant that efficiently crosses the blood-brain barrier in mice, to test PRE variants in the mouse CNS. We delivered 1×10^{11} vg of CMV-eGFP–NLS containing either no PRE, a full-length Woodchuck hepatitis virus PRE (WPRE) sequence, or a truncated WPRE[27] into 8-week-old mice by retro-orbital injection, and harvested brain tissue for imaging after a 3-week incubation. W3 increased PHP.B-delivered GFP–NLS expression levels in the brain ~19-fold compared to no regulatory sequence (Fig. 2a–2c). This increase in payload gene expression was comparable to the increase from using the full-length WPRE sequence (20-fold; Fig. 2a–2c), but W3 is 350 bp smaller than full-length WPRE.

Although the tendency of the CMV promoter to be silenced over time *in vivo* may be beneficial for some genome editing applications by minimizing off-target editing opportunities[19,28,29], we chose to avoid silencing to maximize editing efficiency in this initial study. The Cbh promoter is a ubiquitous, constitutive promoter that is less sensitive to silencing *in vivo* than the CMV promoter[30]. All base editor AAV constructs therefore contained the truncated W3 sequence, Npu intein, and Cbh promoter, which we refer to hereafter as v3 AAV. To optimize split-base editor AAV configurations, we transduced murine 3T3 cells with dual v3 AAV-PHP.B encoding split-CBE3.9 and a validated sgRNA targeting the mouse *DNMT1* locus[22]. A dose of 2×10^{10} viral genomes (vg) AAV total per well of 50,000 NIH 3T3 cells, using a 1:1 ratio of the two AAVs, resulted in 1.7±0.73% C•G-to-T•A editing at the *DNMT1* locus. Replacing CBE3.9 with the NLS- and codon-

optimized CBE3.9max to generate v4 AAV-CBE3.9max improved C•G-to-T•A editing efficiency to 4.1±2.2%, a 2.4-fold increase relative to v3 AAV CBE3.9 (Fig. 2d and 2e).

After optimizing PRE, promoter, NLS, and codon usage, we tested the impact of different guide RNA placements and orientations within the AAV genome. Guide RNA transcription efficiency is known to be sensitive to proximity and orientation relative to AAV ITRs[31]. Moving the U6-sgRNA cassette to the 3' end of the viral genome and reversing its orientation[31], yielding v5 AAV, improved C•G-to-T•A editing efficiency a further 5.6-fold relative to v4 AAV, for a total 14-fold total improvement compared to the initial v3 AAV constructs (23±5.2% for v5 AAV-CBE3.9max versus 1.7±0.73% for v3 AAV-CBE3.9). We repeated these experiments at a 10-fold higher virus dose, 2×10^{11} vg per well, and observed 4-fold higher C•G-to-T•A editing efficiency for v5 AAV compared to v3 AAV, and 1.5-fold higher editing for v5 AAV compared to v4 AAV (14±4.8% for v3 AAV-CBE3.9, 37±18% for v4 AAV-CBE3.9max, and 56±12% for v5 AAV-CBE3.9max) (Fig. 2d and Fig. 2e). Based on these results, we used CBE3.9max and ABEmax in the optimized v5 AAV architecture, referred to hereafter as v5 AAV-CBE or v5 AAV-ABE, for all subsequent experiments. We note that v5 AAV-ABE genomes contain an sgRNA cassette only on the C-terminal half due to size constraints, while v5 AAV-CBE genomes contain sgRNA cassettes on both halves.

Next we characterized the performance of the optimized AAV split-intein base editor constructs *in vivo*. AAV9 is reported to transduce tissues including liver, skeletal muscle, heart, and CNS[32–34]. We generated dual AAV9 particles in the v5 AAV architecture encoding the optimized split CBE3.9max (Fig. 2d) or ABEmax base editors (Supplementary Fig. 2), together with a guide RNA programmed to install a point mutation in *DNMT1*, resulting in A8T for CBE3.9max, or a silent mutation for ABEmax. Importantly, removal of the N-terminal 290 amino acids of DNMT1 has been shown to have minimal functional impact[35], and *DNMT1* itself acts redundantly with *DNMT3a* in the mammalian brain[36]. We therefore do not anticipate *DNMT1* base editing to incur a fitness penalty. We performed systemic (retro-orbital) injections of v5 AAV9-CBE or v5 AAV9-ABE in 6- to 9-week-old C57BL/6 mice. Four weeks after injection of 2×10^{12} vg total per mouse, we measured *DNMT1* editing in the heart, skeletal muscle, brain, liver, lung, kidney, spleen, and reproductive organs. Following a single dual-AAV injection, both split-intein ABE and CBE AAVs resulted in substantial whole-organ base editing of heart (CBE: 15±3.8% C•G-to-T•A editing efficiency in unsorted cells; ABE: 20±1.4% A•T-to-G•C editing efficiency in unsorted cells) skeletal muscle (CBE: 4.4±2.4%, ABE: 9.2±4.0%), and liver (CBE: 21±17%; ABE: 38±2.9%) (Fig. 3a and 3b), three organs that are reported to be transduced by AAV9. Consistent with the previously reported intravenous transduction profile of AAV9[37], we saw little editing in lung, kidney, spleen, and reproductive organs, and no detectable editing in harvested sperm (Supplementary Fig. 3). Together, these results establish that AAV9 delivery of split-intein CBE and ABE enables efficient *in vivo* base editing in tissues known to be transduced by AAV9.

A recent study by Kim and coworkers reported AAV-mediated delivery of ABE split by *trans*-mRNA splicing[8]. To directly compare the efficiency of AAV-delivered base editors reconstituted through split intein-mediated splicing, versus *trans*-mRNA splicing, we generated *trans*-mRNA splicing constructs with the *DNMT1*-targeting sgRNA and Cbh

promoter. Notably, in side-by-side comparisons measuring base editing in three tissues, split intein-spliced v5 AAV-ABE on average provided 4.5-fold higher base editing efficiencies than trans-RNA-spliced ABE (Fig. 3c). These results suggest that intein-mediated base editor protein splicing is more efficient than base editor mRNA trans-splicing. This efficiency difference may arise from the requirements of AAV genome concatamerization[38] followed by transcription and splicing of the ITR sequences, which have been reported to destabilize pre-mRNA[39], for successful *trans*-mRNA splicing.

Notably, base editing efficiencies in heart and skeletal muscle from split-intein AAV9 constructs (Fig. 3) are comparable to or higher than gene rescue efficiencies reported to improve phenotypes in DMD animal models[40,41], and editing in the liver is above the correction thresholds required for phenotypic improvement in several inborn errors of metabolism[42–44]. These findings suggest that the split-AAV base editor systems reported here may be suitable for developing treatments to correct animal models of human genetic diseases. We further note that these constructs have been optimized for general editing efficiency, and not for application-specific improvements including tissue- or cell type-specific promoters, which could further improve specificity and activity in therapeutically relevant cells. Tissues that are not well-transduced by intravenous AAV9 injections may be transduced by other existing AAV variants, such as AAV4 transduction of the lung[45], or by different delivery routes, such as AAV9 transduction of kidney cells by retrograde ureteral infusion[46].

Recently, Villiger and coworkers developed an intein-split *S. aureus* CBE[24]. To compare those constructs to the v5 constructs described in this study, we generated a v5 *S. aureus* CBE using intein-split SaBE3.9max, which has the same NLS- and codon optimizations as the *S. pyogenes* Npu-BE3.9max construct, and cloned it into our v5 AAV architecture. We then packaged dual AAV genomes in AAV8 with an sgRNA designed to generate the *PCSK9* W8X mutation[31], injected either 1×10^{11} or 1×10^{12} total vg per animal retro-orbitally into 3-week-old mice, and harvested liver tissue for high-throughput sequencing 4 weeks after injection. The Villiger constructs were modified only by replacement of the liver-specific P3 promoter with Cbh, and the *Pah*-targeting guide with *PCKS9* W8X. At the higher dose, the constructs performed comparably (v5 AAV saCBE: 20±0.9% W8X-encoding alleles; Villiger saCBE: 18±1.6% W8X-encoding alleles). At the lower dose, however, we observed no reduction in editing by the v5 AAV saCBE constructs (25±6.0% W8X alleles) but a substantial reduction in the editing efficiency of the Villiger constructs (8.2±3.2% W8X alleles) (Supplementary Fig. 3c). We conclude that the higher 1×10^{12} vg dose reaches an editing ceiling due to processes extrinsic to the base editor, such as host DNA repair processes or cell state-specific factors. At the lower dose of the Villiger constructs, the base editor itself is limiting. These results demonstrate that the v5 AAV saCBE constructs can outperform the corresponding constructs developed by Villiger and coworkers.

Base editing in CNS by split-intein CBE and ABE AAV

The above results establish an *in vivo* CBE and ABE delivery solution for somatic tissues transduced following systemic AAV injection. Delivery to the central nervous system (CNS),

however, is especially challenging. Although AAV9 has been reported[47] to cross the blood-brain barrier and transduce CNS cells, we observed minimal editing in the brain following adult retro-orbital injection (Fig. 3). To enable *in vivo* base editing of cells in the CNS, we explored three complementary approaches. First, we performed neonatal cerebroventricular (P0 ICV) injections. Similar to intrathecal injections currently used to deliver nusinersin to treat spinal muscular atrophy (SMA) patients[48], ICV injections are direct injections into cerebrospinal fluid. Second, we performed retro-orbital injections in six-week-old mice using split-intein base editor AAV based on PHP.eB, a laboratory-evolved AAV9 variant with improved ability to penetrate the blood-brain barrier in C57BL/6 mice[49–51]. Finally, we performed subretinal injections to directly transduce retinal tissue, given that AAV-mediated retinal transduction has already been shown to treat ocular disorders[11].

For all CNS delivery experiments, we combined dual split-intein CBE or ABE v5 AAV targeting *DNMT1* together with an AAV encoding a Cbh promoter-driven GFP fused to a nuclear membrane-localized Klarsicht/ANC-1/Syne-1 homology (KASH) domain[22] to enable FACS isolation of cells with GFP-positive nuclei. Sorting for GFP-positive cells enriches cell types that are transducible by AAV and that can transcribe genes from the Cbh promoter. This enrichment is especially useful in the CNS, where the heterogeneity of interspersed cell types limits enrichment from physical dissection alone. For example, in the cerebellum, only Purkinje neurons, comprising less than 1% of total cerebellar tissue[52,53], are well-transduced by known AAV variants at P0[54,55]. These neurons, however, are critically important as their degeneration causes a number of cerebellar ataxias[56,57]. FACS isolation facilitates quantification of editing in this sparse population, as shown by comparison of editing among sorted and unsorted cell populations (Fig. 4).

To determine optimal AAV variants for P0 ICV injections, we co-injected 4×10^{10} vg total of v5 AAV-CBE with 1×10^{10} vg of KASH–GFP (Fig. 4a). We tested four AAV variants that we hypothesized would efficiently transduce CNS cells following these neonatal direct brain injections: AAV8 and AAV9, which have both been reported to transduce neurons following P0 injections[54], and laboratory-evolved PHP.B and PHP.eB AAV variants[26,49], which efficiently transduce CNS tissue in older mice. Measurements of GFP-positive nuclei by flow cytometry showed that in cortical tissue, transduction percentages varied from 43±2.2% (AAV8) to 65±4.4% (PHP.eB). In cerebellar tissue, none of the four serotypes efficiently transduced cells (AAV8: 0.8±0.4%; AAV9: 2.7±0.7%; PHP.B: 1.6±0.2%; PHP.eB: 2.5±0.5%) (Fig. 4b). The low transduction in cerebellum is consistent with previous reports that Purkinje neurons represent nearly all cerebellar neurons transduced following P0 injections[54,55,58]. To confirm that transduced cerebellar cells were Purkinje neurons, we injected *L7-GFP* mice, which express cytoplasmic GFP in Purkinje neurons, with an mCherry-expressing AAV9 construct, and observed robust transduction only in GFP-positive cells (Supplementary Fig. 4a and 4b). Importantly, most Purkinje neurons were transduced, suggesting that GFP-positive nuclei in Fig. 4b reflect a relatively large and unbiased sample of the overall Purkinje cell population. Taken together, these results suggest that all four variants transduce CNS cells with comparable efficiency.

Next, we sequenced cerebellar and cortical tissue. In cortex, we found that all four tested AAV variants mediated comparable and efficient C•G-to-T•A base editing among GFP-

positive cells (65–70% base editing), as well as among unsorted cells (32–50% base editing) (Fig. 4c). In cerebellum, all four AAV variants again resulted in comparable and efficient base editing (Fig. 4c), resulting in 35–52% editing among GFP-positive cells. Since Purkinje neurons form the vast majority of transduced cerebellar cells[54,55,58] but represent only a small percentage of cerebellar tissue, base editing in unsorted cerebellar tissue was inefficient as expected, ranging from 0.52% (AAV8) to 2.5% (AAV9).

Having demonstrated cytosine base editing in the brain with AAV-CBE, we next tested adenine base editing with AAV-ABE. Since all AAV variants tested produced similar CBE3.9max base editing efficiencies, we characterized P0 ICV injections of v5 AAV-ABE using AAV9. We observed that AAV9-delivered split-intein ABE edited cortex with high efficiency (87±4.0% A•T-to-G•C editing among GFP-positive cells; 43±9.1% editing among unsorted cells) and cerebellum (64±5.6% among GFP-positive cells; 1.3±0.5% among unsorted cells, consistent with the small percentage of Purkinje neurons in cerebellum) (Fig. 4d).

Although direct CNS injections resulted in robust base editing in the brain, we also sought to determine whether peripheral delivery of AAV via intravenous injection might efficiently edit the CNS, since intravenous injections offer substantial convenience, cost, and safety advantages. We injected 4×10^{12} vg of PHP.eB encoding v5 AAV-CBE mixed with 2×10^{11} vg GFP-KASH retro-orbitally into nine-week old mice (Fig. 4e). After 3–4 weeks, we harvested and sorted brain tissue. We observed highly efficient C•G-to-T•A base editing in cortex (74±1.2% among GFP-positive cells, and 59±3.0% among unsorted cells) and cerebellum (70±2.6% among GFP-positive cells, and 35±3.0% among unsorted cells; Fig. 4f). These data indicated that, in contrast to P0 ICV injection, intravenous injection of PHP.eB AAV in adult mice results in robust base editing in unsorted cerebellar tissue. Unlike the restrictive tropism observed at P0, in adult mice retro-orbital injection of PHP.eB transduces several cell types in cerebellum including granule cells and Olig2^{+} oligodendrocytes[26]. This broadened tropism could be due to injection route differences or expression differences over time in proteins that mediate AAV transduction. Collectively, these findings establish high-efficiency cytosine and adenine base editing in the central nervous system of a mammal.

In vivo base editing of retinal cells

Genome editing approaches to treating inherited ocular disorders are of special interest given the accessibility of the eye, its immune-privileged status, and the prevalence and impact of congenital blindness. We therefore tested the ability of subretinal injections of v5 AAV-ABE or v5 AAV-CBE to efficiently base edit photoreceptors and other retinal cells. We bred rhodopsin-Cre mice, which express Cre only in retinal rod photoreceptor cells, to Ai9 mice[59] to generate mice that express tdTomato only in rod photoreceptor cells. We performed subretinal injections of v5 AAV-CBE or v5 AAV-ABE targeting *DNMT1* in two-week old mice (Fig. 5a). We tested two AAV variants which have been shown to transduce retinal tissue: PHP.B[26], which performs similarly to AAV9/PHP.eB above in P0 injections, and Anc80, which contains a computationally reconstructed ancestral AAV capsid sequence and

has previously been shown to transduce rods more efficiently than AAV8[60]. PHP.B-Cbh-KASH–GFP or Anc80-Cbh-KASH–GFP was co-injected as a marker for transduced cells.

Three weeks post-injection, we sorted retinal cells into GFP+/tdTomato+ (transduced rods), GFP+/tdTomato- (marker transduced non-rods), GFP-/tdTomato+ (unmarked rods), or double-negative (unmarked non-rods) cells. PHP.B-KASH–GFP transduced 65±2.8% of rods and 9.6±1.4% of non-rods, while a 6-fold lower dose of Anc80-KASH–GFP transduced cells much less efficiently (Fig. 5b). When delivered at the same dose (5×10^9 vg), both PHP.B and Anc80 showed comparable transduction efficiency in the retina, and the majority of cells transduced by both variants were photoreceptors (Fig. 5c). Both PHP.B and Anc80 AAV efficiently delivered split-intein base editors into retinal cells, with PHP.B-mediated v5 AAV-CBE resulting in 48±5.9% C•G-to-T•A editing among GFP$^+$/tdTomato$^+$ rod photoreceptors (19±8.7% among all tdTomato-positive rods), and Anc80-mediated v5 AAV-ABE resulting in 37±22% A•T-to-G•C editing among GFP$^+$/tdTomato$^+$ rod photoreceptors (26±16% editing among all rod photoreceptor cells) (Fig. 5d–5f). These editing efficiencies, even among unsorted PHP.B-transduced rod photoreceptors, are similar to the frequencies of wild-type alleles required to improve retinal function in mosaic *Pde6b* mutant mice[61]. The editing efficiencies we observed are also comparable to those reported in preclinical data for EDIT-101, a single-vector AAV treatment for Leber congenital amaurosis that delivers Cas9 nuclease[62], suggesting that dual-vector AAV co-transduction in retinal tissue can achieve therapeutically relevant editing efficiencies.

Interestingly, although ABE delivery generated very few indels in retinal cells, consistent with previous results from cultured cells[4], and both ABE and CBE delivery in non-retinal tissues in the experiments described above generally resulted in base edit:indel ratios >10:1 (Supplementary Table 1), CBE delivery to retinal cells generated substantial indels, with base edit:indel ratios between 2:1 and 1:1 and indel percentages up to 34%. Despite the substantial frequency of indels, there was little overlap between indel-containing and base-edited alleles. Excluding indel-containing reads did not reduce the number of reads with C•G-to-T•A editing (Supplementary Fig. 5a and 5b), indicating that base edited alleles in general do not contain indels. These observations suggest that CBE-mediated indels in retinal cells occur through uracil excision pathways that are mutually exclusive with pathways that lead to cytosine base editing outcomes, or that base edited or indel-containing products are poor substrates for subsequent indel-generating or base editing processes, respectively.

In vivo correction of a causal Niemann-Pick mutation in mouse CNS

Integrating the above developments, we applied AAV-mediated *in vivo* base editor delivery to correct a mutation associated with human disease in the CNS of an animal. *NPC1* mediates intracellular lipid transport, and loss-of-function mutations cause Niemann-Pick type C (NPC) disease, a neurodegenerative ataxia. *NPC1* c.3182T>C (encoding Ile1061Thr) is the most prevalent mutation in humans that causes NPC disease[63,64]. Previous work suggests that Niemann-Pick disease is primarily a CNS disorder; genetic deletion of *Npc1* in the CNS alone causes Niemann-Pick disease in mice[65], while expression of wild-type *Npc1* in the CNS alone prevents the disease[66,67]. Furthermore, deletion of *Npc1* in Purkinje

neurons alone causes motor impairment[68]. Chimeric mouse studies suggest that the death of Purkinje neurons is cell-autonomous and therefore amenable to mosaic rescue[69]. $Npc1^{I1061T}$ homozygous mice develop ataxia and have a reduced lifespan of approximately 17 weeks[64], while chimeric mice with 15–32% wild-type alleles show modest but detectable increases in lifespan and reduced ataxia.[69]

To test if base editing of *Npc1* c.3182T>C in the CNS might extend lifespan, we injected P0 $Npc1^{I1061T}$ (c.3182T>C) homozygous mice with 4×10^{10} or 1×10^{11} vg total AAV9 encoding v5 AAV-CBE (2×10^{10} or 5×10^{10} vg of each AAV half) targeting the *Npc1* I1061T mutation and 1×10^{10} vg of KASH–GFP, which we refer to as low dose and high dose, respectively. Cytosine base editing at this site should directly revert the 3182T>C mutation (Fig. 6a). Although we found no difference in lifespan between low-dose and untreated mice (Fig. 6b), high-dose mice survived 9.2% longer than untreated mice (Fig. 6b; median survival increases from 102.5 to 112 days, $\chi^2= 5.358$, df=1, p=0.02 by Mantel-Cox test). Given the modest lifespan increase, we treated a second cohort of five $Npc1^{I1061T}$ mice using retro-orbital injections of 3×10^{12} vg v5 PHP.eB-CBE and 1×10^{12} vg AAV9-CBE at P30-P40. Consistent with the results of the first cohort, this second treated cohort survived 10% longer than untreated mice (Supplementary Fig. 6a; median survival increases from 109 to 120 days, $\chi^2= 5.911$, df=1, p=0.015 by Mantel-Cox). Taken together, these findings suggest that *in vivo* AAV-delivered base editing to correct *Npc1* c.3182T>C modestly extends the lifespan of the treated mice.

To determine if v5 AAV9-CBE injection increases the number of surviving Purkinje neurons, we compared a cohort of age-matched injected and untreated mice at P98-P105, close to the lifespan of the untreated mice. In agreement with the observed lifespan extension, injection of AAV9 AAV-CBE increases the number of surviving Purkinje neurons, from 24% of wild-type to 38% of wild-type (uninjected, 5.1±1.2 Purkinje neurons per mm of Purkinje cell layer; injected, 8.0±0.8 PCs/mm; wild-type, 21.1±5.5 PCs/mm; uninjected vs. injected, p=0.03) (Fig. 6c). Quantitatively similar increases in Purkinje cell survival mediated by small molecules in $Npc1^{-/-}$ mice have previously been associated with lifespan increases similar to those we observed[70]. These results demonstrate that AAV-mediated CNS base editing of *Npc1* increases the survival of Purkinje neurons to an extent consistent with the lifespan increase of the treated mice. To further probe the possibility that *Npc1* base editing improves cellular markers of NPC1 disease and to determine whether the CBE-mediated mosaic rescue might provide systemic benefits, we examined CD68^{+} reactive microglia, a measure of CNS inflammation[67,71]. We quantified the density of CD68^{+} cells and total CD68^{+} tissue area in mice injected with AAV9 AAV-CBE, finding modest decreases in CD68^{+} tissue area in agreement with the modest increase in Purkinje cell survival (Fig. 6d, decrease from 19.9±0.05% to 16.7±0.08%; p=0.005. Single-channel images included in Supplementary Fig. 7a). Although CD68^{+} cell density decreased from 913±26 to 850±30 cells/mm^2, this difference was not statistically significant (Supplementary Fig. 7b, p=0.15).

Finally, we euthanized mice from the survival cohort at the onset of morbidity to harvest brain tissue for high-throughput DNA sequencing, and sorted GFP-positive cortical and cerebellar nuclei as described above (Fig. 4). In mice given a low dose of v5 AAV-CBE, the

Npc1 c.3182T>C mutation was corrected with 31±16% efficiency in unsorted cortical nuclei, and in 46±22% of GFP-positive nuclei. In cerebellum, we observed editing of 0.4±0.5% in unsorted tissue, and 11±8.4% in GFP-positive nuclei, which correspond to the critical Purkinje cell population that must be edited to treat NPC disease. In high-dose mice, we observed cortical editing of 48±8.2% and 81±3.7% in unsorted and sorted nuclei, respectively, and target cerebellar editing of 0.3±0.2% and 42±14% of unsorted and sorted nuclei, respectively (Fig. 6e). In all cases, C-to-T editing without bystander edits or indels was predominant among edited alleles; over 94% of edited alleles precisely correct the c. 3182T>C mutation and encode the wild-type allele (Fig. 6e; indels reported in Supplementary Table 1). We also determined whether off-target editing might occur in the sorted cerebellar and cortical nuclei. We identified candidate loci using two methods: we used CRISPOR, a bioinformatic method to predict off-target sites with Cas9 activity, and we empirically determined off-target Cas9 loci using CIRCLE-seq on gDNA harvested from the liver of an untreated *Npc1*[I1061T] mouse. We then performed amplicon sequencing to confirm editing at eight total candidate loci identified by either method. We observed only a single confirmed off-target site, an intronic sequence in *Epas1* >3kb away from the nearest exonic sequences, which was edited at a low efficiency of 0.3±0.05% (Supplementary Fig. 8).

Previous work with mosaic mice has shown that approximately 15–32% wild-type *Npc1* alleles are required for modest but measurable phenotypic improvement and lifespan extension[69]. Since the above data suggest ~11% Purkinje cell editing in low-dose mice with no lifespan extension, and ~42% Purkinje cell editing in high-dose mice with modest but significant lifespan extension, our results are wholly consistent with the modest lifespan gains observed in mosaic mice with similar proportions of wild-type alleles[69].

We note that unedited cells may have degenerated, and thus editing levels in sequenced tissue represent upper limits of the initial percentage of edited cells. To minimize the effect of degeneration on the frequency of edited cells, we measured base editing in heterozygous *Npc1*[I1061T/+] mice, which do not show NPC disease phenotypes, following high-dose P0 injections. At P29, we found 31±5.8% of GFP-positive cerebellar nuclei were edited, which increased to 54±10% at P110. In sorted cortical nuclei, the percent of edited cells increased from 59±5.4% to 82±7.2% (Supplementary Fig. 9a), suggesting that C•G to T•A editing continues for more than four weeks after P0 injection. To test whether CBE is chronically expressed, we injected *Npc1*^{+/+} mice with v5 AAV-CBE at P0 and harvested brains at P110 for staining against Cas9 and GFP. We observed expression of both Cas9 and GFP at P110 in cerebellar and cortical tissue (Supplementary Fig. 9b and 9c), suggesting that, consistent with previous studies, AAV mediates long-term neuronal transgene expression. Although the above data are consistent with a prolonged editing activity window, and though *Npc1*^{+/−} heterozygotes do not have any cellular markers of disease[67], we cannot rule out the possibility that the apparent continued editing in heterozygotes may simply be the result of a survival advantage in edited cells.

These results establish that dual AAV split-intein base editor delivery in Niemann-Pick type C mice directly corrects a substantial fraction of pathogenic alleles in the CNS. Together, these results demonstrate base editing to treat an animal model of a human CNS disease.

Discussion

This study describes an optimized dual AAV system that delivers split-intein cytosine and adenine base editors, resulting in therapeutically relevant *in vivo* genome editing efficiencies following injection of ~10^{13}-10^{14} vg/kg, a dosage comparable to those currently used in human gene therapy trials[32]. The optimizations described above greatly improve the efficiency of AAV-encoded base editors and may also be useful to other AAV-based systems for the delivery of genome editing agents[8,24]. Many somatic cell types of therapeutic and scientific interest can be efficiently transduced with known AAV variants, including hematopoetic cells[72], liver[73], sensory organs[11], and CNS[32], suggesting that this work may facilitate a broad range of studies in animal models of many human genetic diseases. Finally, we tested different injection routes to deliver AAV-packaged split-base editors in postnatal mice, and demonstrate efficient base editing in brain and retina, enabling causal gene correction of Niemann-Pick type C disease. Previous work has shown that gene augmentation by AAV9-delivered *Npc1* significantly increases lifespan in *Npc1*$^{-/-}$ mice[71,74,75]. *Npc1* gene augmentation appears to improve lifespan more than the split-editor constructs described here, although delivery efficiency appears similar, potentially due to gene augmentation producing functional *Npc1* in all transduced cells without requiring additional mechanistic steps. Further improvements to the base editors and AAV architecture may improve phenotypic rescue in this setting.

The mouse studies described here use AAV injections of no more than 4×10^{12} vg per 20-g animal, which corresponds to a maximum dose of 2×10^{14} vg/kg, consistent with the maximum dosages delivered intravenously in non-human primate studies[76] and clinical trials[32] for CNS delivery. Notably, in the eye, subretinal injections of our optimized base editor AAVs achieve genome editing efficiencies comparable to those of preclinical delivery systems optimized for retinal editing[62]. Intravenous v5 AAV injections also achieve therapeutically relevant editing levels in liver, muscle, and cardiac tissue. The viral base editing systems developed in this study therefore are suitable for testing base editing strategies in animal models of human disease, a key step in advancing base editing towards human therapeutic application. AAV optimization (Fig. 2) reduced the viral dose required for efficient base editing to amounts known to be tolerated by humans, enabling more practical and therapeutically relevant editing in animal models of human genetic diseases compared to the much higher doses previously used in trans-splicing mRNA viral vectors[8].

While we initially anticipated that the requirement of simultaneous transduction by two viruses would sharply lower editing efficiencies, the surprisingly high overall *in vivo* editing efficiencies we observed even among unsorted cells (for example, up to 59% of cortex), together with similar levels of transduction of single AAVs expressing GFP as levels of edited cells that required dual AAV transduction (Fig. 4b) strongly suggest that transducible cells are particularly amenable to transduction by multiple AAVs. Editing efficiency may be further increased by tissue-specific optimization such as selection of a delivery route that biases AAV concentrations towards relevant tissues, such as hepatic artery injections to transduce liver[77], and tissue-specific promoter and terminator variation to enhance expression in specific cell types.

The split-intein base editor delivery system developed here brings the strengths of base editing, including high editing efficiency, minimization of unwanted byproducts arising from double-stranded DNA breaks, and compatibility with post-mitotic somatic cells[2,9], to *in vivo* settings in the diverse tissue types that are well-transduced by natural or engineered AAVs. The split-intein dual AAV approach described here may also facilitate the *in vivo* delivery of genes that are too large for a direct gene augmentation approach.

Methods

Molecular Biology

All expression vectors used for HEK293T transfection were generated by Gibson cloning. All sgRNA constructs were generated by ligation of annealed oligos into pFYF1320 modified to contain a BsmBI dummy spacer that leaves 5'-CACC and 5'-CAAA overhangs compatible with general sgRNA cloning techniques (e.g. https://www.addgene.org/crispr/zhang/). AAV vectors were generated by Gibson cloning of PCR-amplified inserts into restriction enzyme digested backbones.

Cell culture

HEK239T/17 (ATCC CRL-11268) and 3T3 cells (ATCC CRL-1658) were maintained in DMEM (Thermo Fisher 10569044) supplemented with 10% (v/v) fetal bovine serum (Thermo Fisher), at 37 °C with 5% CO2. Cells were verified to be free of mycoplasma by ATCC upon purchase, and periodically during culture. For cell culture experiments, transfections of independently maintained cell lines, or different passages of the same cell line, were considered biologically independent measurements.

HEK293T and 3T3 transfection and genomic DNA preparation

HEK293T cells were seeded into 48-well Poly-D-Lysine-coated plates (Corning 354509) at 30,000 cells / well. One day after plating, cells were transfected by Lipofectamine 2000 (Thermo Fisher) according to the manufacturer's directions with 1 µg DNA in a 1:1 molar ratio of base editor and sgRNA plasmids, plus 10 ng of fluorescent protein expression plasmid as a transfection control. Cells were cultured for 3 days before genomic DNA was extracted by replacement of culture media with 100 µL lysis buffer (10 mM Tris-HCl, pH 7.5, 0.05% SDS, 25 µg/mL proteinase K (NEB) and 37 °C incubation for 1 hour. Proteinase K was inactivated by 30-minute incubation at 80 °C. 3T3 cells were transfected using the same procedure at 50,000 cells / well. For AAV experiments, 10^{10}-10^{11} vg were added to wells containing 50,000 3T3 cells, resulting in MOIs of 2×10^5-2×10^6 vg/cell.

Western blotting

HEK293T cells were seeded into 12-well plates at 125,000 cells per well. Cells were transfected as described above with all amounts scaled up 3x. For conditions with transfection of only one split-half, EGFP-expressing plasmid was used to normalize the amount of DNA used. 3 days after transfection, cells were gently lifted and triturated by pipetting PBS across the well surface. 10% of the volume was removed for HTS analysis, and the remaining cells were washed with ice-cold PBS, and incubated on ice for 15 minutes in lysis buffer (300 mM NaCl, 50 mM Tris pH 8, 1% IGEPAL 0.5% deoxycholic acid, 10

mM MgCl) plus 25 U/mL salt active nuclease (Arcticzymes 70910–202) to reduce lysate viscosity and cOmplete EDTA-free protease inhibitor cocktail (Roche). After 10 minutes, SDS and EDTA were added to 0.5% and 1 mM, respectively, and lysates were rocked an additional 15 minutes at 4 °C before clarification by centrifugation at 14,000 g for 15 minutes at 4 °C. Lysates were normalized using BCA (Pierce BCA Protein Assay Kit), and 2.5 mg of reduced protein was loaded onto each gel lane. Transfer was performed with an iBlot 2 dry blotting system (Thermo Fisher) using the following program: 20 V for 1 min, then 23 V for 4 min, then 25 V for 2 min for a total transfer time of 7 minutes. Blocking was performed at room temperature for 30 minutes with block buffer: 1% BSA in TBST (150 mM NaCl, 0.5% Tween-20, 50 mM Tris-Cl, pH 7.5). Membranes were then incubated in primary antibody diluted in block buffer at 4 °C overnight. After a wash step, secondary antibodies diluted in TBST were added. Membranes were washed again and imaged using a LI-COR Odyssey. Wash steps were 3× 5 minute washes in TBST. Primary antibodies used were rabbit anti-GAPDH, 1:1000 (Cell Signaling Technologies D16H11); rabbit anti-HA, 1:1000 (Cell Signaling Technologies C29F4), mouse anti-FLAG 1 μg/mL (clone M2, Sigma F1804). LI-COR IRDye 680RD goat anti-rabbit (#926–68071) and goat anti-mouse (#926–68070) secondary antibodies were used at 1:10,000–1:20,000 dilutions.

High-throughput sequencing and data analysis

Genomic DNA was amplified by qPCR using Phusion Hot Start II DNA polymerase with use of SYBR gold for quantification. 3% DMSO was added to all gDNA PCR reactions. To minimize PCR bias, reactions were stopped during the exponential amplification phase. 1 uL of the unpurified gDNA PCR product was used as a template for subsequent barcoding PCR (8 cycles, annealing temperature 61 °C). Pooled barcoding PCR products were gel-extracted (Min-elute columns, Qiagen) and quantified by qPCR (KAPA KK4824) or Qubit dsDNA HS assay kit (Thermo Fisher). Sequencing of pooled amplicons was performed using an Illumina MiSeq according to the manufacturer's instructions. All oligonucleotide sequences used for gDNA amplification are provided in Supplementary Table 1.

Initial de-multiplexing and FASTQ generation were performed by bcl2fastq2 running on BaseSpace (Illumina) with the following flags: --ignore-missing-bcls --ignore-missing-filter --ignore-missing-positions --ignore-missing-controls --auto-set-to-zero-barcode-mismatches --find-adapters-with-sliding-window --adapter-stringency 0.9 --mask-short-adapter-reads 35 --minimum-trimmed-read-length 35. Alignment of fastq files and quantification of editing frequency was performed by CRISPResso2 in batch mode with the following flags: --min_bp_quality_or_N 20 --base_editor_output -p 2 -w 20 -wc −10. For PCKS9 experiments, the total number of reads encoding Trp 8 to STOP (TAA, TGA, and TAG) were summed and divided by the number of aligned reads.

AAV production

AAV production was performed as previously described[26] with some alterations. HEK293T/17 cells were maintained in DMEM/10% FBS without antibiotic in 150mm dishes (Thermo Fisher 157150), and passaged every 2–3 days. Cells for production were split 1:3 1 day before PEI transfection. 5.7 μg AAV genome, 11.4 μg pHelper (Clontech), and 22.8 μg rep-cap plasmid were transfected per plate. 1 day after transfection, media was

exchanged for DMEM/5% FBS. 3 days after transfection, cells were scraped with a rubber cell scraper (Corning), pelleted by centrifugation for 10 minutes at 2000 g, resuspended in 500 μL hypertonic lysis buffer per plate (40 mM Tris base, 500 mM NaCl, 2 mM MgCl$_2$ with 100 U/mL salt active nuclease (Arcticzymes 70910–202), and incubated at 37 °C for 1 h to lyse cells. Media was decanted, combined with a 5x solution of 40% PEG in 2.5 M NaCl (final concentration 8% PEG / 500 mM NaCl), incubated on ice for 2 hours to facilitate PEG precipitation, and centrifuged at 3200 g for 40 minutes. The supernatant was discarded and the pellet resuspended in 500 μL lysis buffer per plate and added to the cell lysate. Incubation at 37 °C was continued for 30 minutes. Crude lysates were either incubated at 4 °C overnight or directly used for ultracentrifugation.

Cell lysates were gently clarified by centrifugation at 2000 g for 10 minutes and added to Beckman Quick-seal tubes via 16-gauge 5" disposable needles (Air-Tite N165). A discontinuous iodixanol gradient was formed by sequentially floating layers: 9 mL 15% iodixanol in 500 mM NaCl and 1x PBS-MK (1x PBS plus 1 mM MgCl$_2$ and 2.5 mM KCl), 6 mL 25% iodixanol in 1x PBS-MK, and 5 mL each of 40% and 60% iodixanol in 1x PBS-MK. Phenol red at a final concentration of 1 μg/mL was added to the 15, 25, and 60% layers to facilitate identification. Ultracentrifugation was performed using a Ti 70 rotor in a Sorvall WX+ series ultracentrifuge (Thermo Fisher) at 58,600 rpm for 2:15 (h:mm) at 18 °C. Following ultracentrifugation, roughly 4 mL of solution was withdrawn from the 40%−60% iodixanol interface via an 18-gauge needle, dialyzed with PBS containing 0.001% F-68, and ultrafiltered via 100-kD MWCO columns (EMD Millipore). The concentrated viral solution was sterile-filtered using a 0.22 μm filter, quantified via qPCR (AAVpro Titration Kit v.2, Clontech), and stored at 4°C until use.

Animals

All experiments in live animals were approved by the Broad Institute and Massachusetts Eye and Ear Institutional and Animal Care and Use Committees. Wild-type C57BL/6 mice were from Charles River (#027). Jackson Labs supplied all transgenic mice: Npc1$^{tm(I1061T)Dso}$ (#027704), Ai9 (#007909), Rhodopsin-iCre (#015850), and L7-GFP (#004690).

Retro-orbital injections

AAV was diluted to 200 μL in 0.9% NaCl (Fresenius Kabi 918610) before injection. Anesthesia was induced with 4% isoflurane. Following induction as measured by unresponsiveness to a toe pinch, the right eye was protruded by gentle pressure on the skin, and a tuberculin syringe advanced, with the bevel facing away from the eye, into the retrobulbar sinus where AAV mix was slowly injected. For assessments of CNS editing, 1×10^{11} vg GFP–KASH virus was added to the injection mix as a transduction marker. gDNA was purified from minced tissue using Agencourt DNAdvance kits (Beckman Coulter A48705) in accordance with the manufacturer's directions.

P0 ventricle injections

Drummond PCR pipettes (5–000-1001-X10) were pulled at ramp and passed through a Kimwipe three times, resulting in a tip size roughly 100 μm. A small amount of Fast Green was added to the AAV injection solution to assess ventricle targeting. The injection solution

was loaded via front-filling using the included Drummond plungers. P0 pups were anesthetized by placement on ice for 2–3 minutes, until they were immobile and unresponsive to a toe pinch. 2 μL of injection mix was injected freehand into each ventricle. Ventricle targeting was assessed by the spread of fast green throughout the ventricles via transillumination of the head.

Nuclear isolation and sorting

Cerebella were separated from the brain with surgical scissors, hemispheres were separated using a scalpel, and the hippocampus and neocortex were separated from underlying midbrain tissue with a curved spatula. Nuclei were isolated from brain tissue as previously described[78]. All steps were performed on ice or at 4 °C. Dissected tissue was homogenized using a glass dounce homogenizer (Sigma D8938) (20 strokes with pestle A followed by 20 strokes with pestle B) in 2 mL ice-cold EZ-PREP buffer (Sigma NUC-101). Samples were incubated for 5 minutes with an additional 2 mL EZ-PREP buffer. Nuclei were centrifuged at 500 g for 5 minutes, and the supernatant removed. Samples were resuspended with gentle pipetting in 4 mL ice-cold Nuclei Suspension Buffer (NSB) consisting of 100 μg/mL BSA and 3.33 μM Vybrant DyeCycle Violet (Thermo Fisher) in 1xPBS, and centrifuged at 500 g for 5 minutes. The supernatant was removed and nuclei were resuspended in 1–2 mL NSB, passed through a 35 μm strainer, and sorted into 200 μL Agencourt DNAdvance lysis buffer using a MoFlo Astrios (Beckman Coulter) at the Broad Institute flow cytometry core. Genomic DNA was purified according to the Agencourt DNAdvance instructions for 200 μL volume.

P14 sub-retinal injections

1 μL of AAV mix for sub-retinal injections consisted of 4×10^9 vg of each split CBE base editor half, and 2×10^9 vg GFP for the PHP.B variant. The Anc80+CBE3.9max mixture was divided equally: 3.3×10^8 vg of each split base editor half, and 3.3×10^8 vg GFP. The Anc80+ABEmax mixture consisted of 4.5×10^8 vg of each split base editor half, and 4.5×10^8 vg GFP. PHP.B or Anc80 GFP alone at 5×10^9 vg/μL was injected into wild-type C57BL/6 mice to assess transduction efficiency. P14 mice were anesthetized by intraperitoneal of ketamine (140 mg/kg) and xylazine (14 mg/kg). Using a microscope for visualization, a small incision was made at the limbus by a 30-gauge needle, and a Hamilton syringe with a 33-gauge blunt-ended needle was used to inject 1 μL of AAV mix. Following injection, mice were placed on a 37 °C warming pad until they recovered.

Retina dissociation and cell sorting

Three weeks post-injection, eyes were enucleated and stored in BGJB medium (Thermo Fisher) on ice as described previously[79]. Retinas were isolated under a fluorescent dissection microscope to record the transfected region and dissociated into single cells by incubation in solution A containing 1 mg/mL pronase (Sigma-Aldrich) and 2 mM EGTA in BGJB medium at 37 °C for 20 minutes. Solution A was gently removed, followed by adding equal amount of solution B containing 100 U/mL DNase I (New England Biolabs), 0.5% BSA, 2 mM EGTA in BGJB medium. Cells were collected and re-suspended in 1xPBS, filtered through a cell strainer (BD Biosciences, San Jose, CA), and sorted using a FACSAriaII (BD Biosciences).

Retinal histology

Mice injected with PHP.B or Anc80 GFP alone were sacrificed 3 weeks post-injection and perfused with 4% paraformaldehyde in 1xPBS. Eyes were dissected and eye cups were embedded in OCT freezing medium. 10 μm Retinal cryosections were cut and stained with DAPI. Images were taken using an Eclipse Ti microscope (Nikon).

Brain Immunohistochemistry

For comparison of PRE sequences, mice were transcardially perfused with PBS followed by 4% PFA. Harvested brains were rotated in 4% PFA at 4 °C overnight for post-fixation. Brains were transferred to 30% sucrose in 1xPBS for cryoprotection and rotated at 4 °C until equilibrated, as assessed by loss of buoyancy. Cryoprotected brains were frozen in a dry ice-ethanol bath and sectioned horizontally on a Leica CM1950 at 20 μm. For analysis of Purkinje neurons and activated microglia, brains were dissected and drop-fixed in 4% PFA overnight on a rotator. Brains were transferred to 1xPBS with 10mM glycine and rotated at 4 °C for at least 24 h. Slices were embedded in 3% agarose for sagittal sectioning on a Leica VT1200 at 20 μm. Midline saggital slices were taken by mounting the agarose blocks containing individual hemispheres on the lateral surface. Only 50 sections were taken to minimize regional variability across animals. For each marker, 3–10 slices per animal were analyzed. The immunostaining procedure was identical for both cases: samples were blocked and permeabilized in 3% BSA (Jackson Immunoresearch) and 0.1% Trition-X 100 in PBS. Samples were incubated in primary antibody at 4 °C overnight, washed three times for 10 minutes each with PBS containing 0.1% Triton-X (PBSTx), incubated with secondary antibody at room temperature for 1 hour, washed 3× 10 minutes with PBSTx, and mounted in ProLong Diamond Antifade with DAPI (Thermo Fisher). In some cases, slides were mounted in ProLong Diamond Antifade (-DAPI) supplemented with 5 μM DRAQ5, a far-red DNA stain, to label DNA. Slides were cured overnight at room temperature before imaging. Care was taken to minimize light exposure at all steps. Primary antibodies used were as follows: chicken anti-GFP, 10 μg/mL (Abcam ab13970); rabbit anti-RFP, 1.6 μg/mL (Rockland 600–401-379); rabbit anti-Calbindin, 0.1 μg/mL. (Cell Signaling Technology D1I4Q); rat anti-CD68, 1 μg/mL (Bio-Rad MCA1957); mouse anti-Cas9, 5 μg/ml (Clone 7A9, Thermo Fisher MA5–23519). Alexa-conjugated goat secondary antibodies (Thermo Fisher) were used at 1:500. Calbindin was imaged using Alexa 647-conjugated secondary antibodies to avoid bleedthrough from virally-delivered GFP. Images were captured and stitched at 10x magnification using a Zeiss Axio Scan.Z1 and included software. Image intensity was kept below 50% saturation to prevent oversaturation.

Image Analysis

Images were analyzed using ImageJ (Fiji), ilastik[80], and CellProfiler[81]. Details and custom ImageJ macros are provided in Supplementary Methods. A subset of images were manually analyzed by a blinded experimenter to validate the accuracy of the final imaging pipelines. Differences between the automated and manual counts were <10%.

Off-target Analysis

CIRCLE-seq was performed as previously described[82]. PCR amplification before sequencing was conducted using PhusionU polymerase, and products were gel-purified and quantified with a KAPA library quantification kit before loading onto an Illumina MiSeq. Data was processed using the CIRCLE-Seq analysis pipeline with parameters: "read_threshold: 4; window_size: 3; mapq_threshold: 50; start_threshold: 1; gap_threshold: 3; mismatch_threshold: 6; merged_analysis: True". The three sites found by CIRCLE-seq analysis were chosen for PCR amplification and high-throughput sequencing. CRISPOR analysis[83] was done and the top five off-target candidates by CFD score were analyzed by amplicon sequencing.

Npc1[I1061T] survival measurements

Npc1 [I1061T] mice were euthanized at the onset of morbidity, defined functionally as profound ataxia leading to an inability to acquire food and water, as evidenced by a low body condition score[84,85] and minimal responsiveness to touch. In all cases, low body condition score preceded profound ataxia. Profound ataxia was the diagnostic criterion for morbundity. The endpoint was designed to minimize suffering while providing accurate survival data. Euthanasia recommendations were made by a blinded veterinary technician. All survival groups were mixed-gender.

Statistical Analysis

Unpaired two-sided t-tests were used to compare immunofluorescence datasets. The logrank (Mantel-Cox) test was used to compare Kaplan-Meier survival curves. All statistical tests were calculated by GraphPad. No corrections were made for multiple comparisons.

Reporting summary

Further information on research design is available in the Nature Research Reporting Summary linked to this article.

Code availability

The custom code used in this study is provided in the Supplementary Information.

Data availability

The data supporting the results in this study are available within the paper and its Supplementary Information. All unmodified reads for sequencing-based data in the manuscript are available from the NCBI Sequence Read Archive, under accession number PRJNA532891. AAV genome sequences are provided in the Supplementary Information. Key plasmids from this work will be available from Addgene (depositor: David R. Liu), and other plasmids and raw data are available from the corresponding author on request.

Supplementary Material

Refer to Web version on PubMed Central for supplementary material.

Acknowledgements

References

1. Landrum MJ et al. ClinVar: public archive of relationships among sequence variation and human phenotype. Nucleic acids research 42, D980–985, doi:10.1093/nar/gkt1113 (2014). [PubMed: 24234437]

2. Rees HA & Liu DR Base editing: precision chemistry on the genome and transcriptome of living cells. Nature reviews. Genetics 19, 770–788, doi:10.1038/s41576-018-0059-1 (2018).

3. Komor AC, Kim YB, Packer MS, Zuris JA & Liu DR Programmable editing of a target base in genomic DNA without double-stranded DNA cleavage. Nature 533, 420–424, doi:10.1038/nature17946 (2016). [PubMed: 27096365]

4. Gaudelli NM et al. Programmable base editing of A*T to G*C in genomic DNA without DNA cleavage. Nature 551, 464–471, doi:10.1038/nature24644 (2017). [PubMed: 29160308]

5. Komor AC et al. Improved base excision repair inhibition and bacteriophage Mu Gam protein yields C:G-to-T:A base editors with higher efficiency and product purity. Sci Adv 3, eaao4774, doi:10.1126/sciadv.aao4774 (2017). [PubMed: 28875174]

6. Koblan LW et al. Improving cytidine and adenine base editors by expression optimization and ancestral reconstruction. Nature biotechnology, doi:10.1038/nbt.4172 (2018).

7. Nishida K et al. Targeted nucleotide editing using hybrid prokaryotic and vertebrate adaptive immune systems. Science 353, doi:10.1126/science.aaf8729 (2016).

8. Ryu SM et al. Adenine base editing in mouse embryos and an adult mouse model of Duchenne muscular dystrophy. Nature biotechnology 36, 536–539, doi:10.1038/nbt.4148 (2018).

9. Yeh WH, Chiang H, Rees HA, Edge ASB & Liu DR In vivo base editing of post-mitotic sensory cells. Nat Commun 9, 2184, doi:10.1038/s41467-018-04580-3 (2018). [PubMed: 29872041]

10. Chadwick AC, Wang X & Musunuru K In Vivo Base Editing of PCSK9 (Proprotein Convertase Subtilisin/Kexin Type 9) as a Therapeutic Alternative to Genome Editing. Arterioscler Thromb Vasc Biol 37, 1741–1747, doi:10.1161/ATVBAHA.117.309881 (2017). [PubMed: 28751571]

11. Russell S et al. Efficacy and safety of voretigene neparvovec (AAV2-hRPE65v2) in patients with RPE65-mediated inherited retinal dystrophy: a randomised, controlled, open-label, phase 3 trial. Lancet 390, 849–860, doi:10.1016/S0140-6736(17)31868-8 (2017). [PubMed: 28712537]

12. Carvalho LS et al. Evaluating Efficiencies of Dual AAV Approaches for Retinal Targeting. Front Neurosci 11, 503, doi:10.3389/fnins.2017.00503 (2017). [PubMed: 28943836]

13. Wu Z, Yang H & Colosi P Effect of genome size on AAV vector packaging. Molecular therapy : the journal of the American Society of Gene Therapy 18, 80–86, doi:10.1038/mt.2009.255 (2010). [PubMed: 19904234]

14. Liu DR, Levy Jonathan M., Wei Hsi Yeh. AAV Delivery Of Nucleobase Editors. United States patent (2017).

15. Truong DJJ et al. Development of an intein-mediated split-Cas9 system for gene therapy. Nucleic acids research 43, 6450–6458, doi:10.1093/nar/gkv601 (2015). [PubMed: 26082496]

16. Zetsche B, Volz SE & Zhang F A split-Cas9 architecture for inducible genome editing and transcription modulation. Nature biotechnology 33, 139–142, doi:10.1038/nbt.3149 (2015).

17. Wright AV et al. Rational design of a split-Cas9 enzyme complex. Proc Natl Acad Sci U S A 112, 2984–2989, doi:10.1073/pnas.1501698112 (2015). [PubMed: 25713377]

18. Zettler J, Schutz V & Mootz HD The naturally split Npu DnaE intein exhibits an extraordinarily high rate in the protein trans-splicing reaction. FEBS letters 583, 909–914, doi:10.1016/j.febslet.2009.02.003 (2009). [PubMed: 19302791]

19. Davis KM, Pattanayak V, Thompson DB, Zuris JA & Liu DR Small molecule-triggered Cas9 protein with improved genome-editing specificity. Nat Chem Biol 11, 316–318, doi:10.1038/nchembio.1793 (2015). [PubMed: 25848930]

20. Stevens AJ et al. Design of a Split Intein with Exceptional Protein Splicing Activity. J Am Chem Soc 138, 2162–2165, doi:10.1021/jacs.5b13528 (2016). [PubMed: 26854538]

21. Shah NH, Eryilmaz E, Cowburn D & Muir TW Extein residues play an intimate role in the rate-limiting step of protein trans-splicing. J Am Chem Soc 135, 5839–5847, doi:10.1021/ja401015p (2013). [PubMed: 23506399]

22. Swiech L et al. In vivo interrogation of gene function in the mammalian brain using CRISPR-Cas9. Nature biotechnology 33, 102–106, doi:10.1038/nbt.3055 (2015).

23. Kim YB et al. Increasing the genome-targeting scope and precision of base editing with engineered Cas9-cytidine deaminase fusions. Nature biotechnology 35, 371–376 (2017).

24. Villiger L et al. Treatment of a metabolic liver disease by in vivo genome base editing in adult mice. Nature medicine 24, 1519–1525, doi:10.1038/s41591-018-0209-1 (2018).

25. Grieger JC & Samulski RJ Packaging capacity of adeno-associated virus serotypes: impact of larger genomes on infectivity and postentry steps. Journal of virology 79, 9933–9944, doi:10.1128/JVI.79.15.9933-9944.2005 (2005). [PubMed: 16014954]

26. Deverman BE et al. Cre-dependent selection yields AAV variants for widespread gene transfer to the adult brain. Nature biotechnology 34, 204–209, doi:10.1038/nbt.3440 (2016).

27. Choi JH et al. Optimization of AAV expression cassettes to improve packaging capacity and transgene expression in neurons. Mol Brain 7, 17, doi:10.1186/1756-6606-7-17 (2014). [PubMed: 24618276]

28. Zuris JA et al. Cationic lipid-mediated delivery of proteins enables efficient protein-based genome editing in vitro and in vivo. Nature biotechnology 33, 73–80, doi:10.1038/nbt.3081 (2015).

29. Rees HA et al. Improving the DNA specificity and applicability of base editing through protein engineering and protein delivery. Nat Commun 8, 15790, doi:10.1038/ncomms15790 (2017). [PubMed: 28585549]

30. Gray SJ et al. Optimizing promoters for recombinant adeno-associated virus-mediated gene expression in the peripheral and central nervous system using self-complementary vectors. Hum Gene Ther 22, 1143–1153, doi:10.1089/hum.2010.245 (2011). [PubMed: 21476867]

31. Ran FA et al. In vivo genome editing using Staphylococcus aureus Cas9. Nature 520, 186–191, doi:10.1038/nature14299 (2015). [PubMed: 25830891]

32. Mendell JR et al. Single-Dose Gene-Replacement Therapy for Spinal Muscular Atrophy. N Engl J Med 377, 1713–1722, doi:10.1056/NEJMoa1706198 (2017). [PubMed: 29091557]

33. Wu Z, Asokan A & Samulski RJ Adeno-associated virus serotypes: vector toolkit for human gene therapy. Molecular therapy : the journal of the American Society of Gene Therapy 14, 316–327, doi:10.1016/j.ymthe.2006.05.009 (2006). [PubMed: 16824801]

34. Duan D Systemic AAV Micro-dystrophin Gene Therapy for Duchenne Muscular Dystrophy. Molecular therapy : the journal of the American Society of Gene Therapy, doi:10.1016/j.ymthe.2018.07.011 (2018).

35. Garvilles RG et al. Dual Functions of the RFTS Domain of Dnmt1 in Replication-Coupled DNA Methylation and in Protection of the Genome from Aberrant Methylation. PloS one 10, e0137509, doi:10.1371/journal.pone.0137509 (2015). [PubMed: 26383849]

36. Feng J et al. Dnmt1 and Dnmt3a maintain DNA methylation and regulate synaptic function in adult forebrain neurons. Nature neuroscience 13, 423–430, doi:10.1038/nn.2514 (2010). [PubMed: 20228804]

37. Inagaki K et al. Robust systemic transduction with AAV9 vectors in mice: efficient global cardiac gene transfer superior to that of AAV8. Molecular therapy : the journal of the American Society of Gene Therapy 14, 45–53, doi:10.1016/j.ymthe.2006.03.014 (2006). [PubMed: 16713360]

38. Duan D, Yue Y & Engelhardt JF Expanding AAV packaging capacity with trans-splicing or overlapping vectors: a quantitative comparison. Molecular therapy : the journal of the American Society of Gene Therapy 4, 383–391, doi:10.1006/mthe.2001.0456 (2001). [PubMed: 11592843]

39. Xu Z et al. Trans-splicing adeno-associated viral vector-mediated gene therapy is limited by the accumulation of spliced mRNA but not by dual vector coinfection efficiency. Hum Gene Ther 15, 896–905, doi:10.1089/hum.2004.15.896 (2004). [PubMed: 15353044]

40. van Putten M et al. Low dystrophin levels increase survival and improve muscle pathology and function in dystrophin/utrophin double-knockout mice. FASEB journal : official publication of the Federation of American Societies for Experimental Biology 27, 2484–2495, doi:10.1096/fj. 12-224170 (2013). [PubMed: 23460734]

41. Li D, Yue Y & Duan D Marginal level dystrophin expression improves clinical outcome in a strain of dystrophin/utrophin double knockout mice. PloS one 5, e15286, doi:10.1371/journal.pone. 0015286 (2010). [PubMed: 21187970]

42. Tuchman M, Jaleel N, Morizono H, Sheehy L & Lynch MG Mutations and polymorphisms in the human ornithine transcarbamylase gene. Hum Mutat 19, 93–107, doi:10.1002/humu.10035 (2002). [PubMed: 11793468]

43. Treacy EP et al. Analysis of Phenylalanine Hydroxylase Genotypes and Hyperphenylalaninemia Phenotypes Using L-[1–13C]Phenylalanine Oxidation Rates in Vivo: A Pilot Study1. Pediatric Research 42, 430, doi:10.1203/00006450-199710000-00002 (1997). [PubMed: 9380432]

44. Hamman K et al. Low therapeutic threshold for hepatocyte replacement in murine phenylketonuria. Molecular therapy : the journal of the American Society of Gene Therapy 12, 337–344, doi: 10.1016/j.ymthe.2005.03.025 (2005). [PubMed: 16043102]

45. Zincarelli C, Soltys S, Rengo G & Rabinowitz JE Analysis of AAV serotypes 1–9 mediated gene expression and tropism in mice after systemic injection. Molecular therapy : the journal of the American Society of Gene Therapy 16, 1073–1080, doi:10.1038/mt.2008.76 (2008). [PubMed: 18414476]

46. Asico LD et al. Nephron segment-specific gene expression using AAV vectors. Biochem Biophys Res Commun 497, 19–24, doi:10.1016/j.bbrc.2018.01.169 (2018). [PubMed: 29407172]

47. Foust KD et al. Intravascular AAV9 preferentially targets neonatal neurons and adult astrocytes. Nature biotechnology 27, 59–65, doi:10.1038/nbt.1515 (2009).

48. Mercuri E et al. Nusinersen versus Sham Control in Later-Onset Spinal Muscular Atrophy. N Engl J Med 378, 625–635, doi:10.1056/NEJMoa1710504 (2018). [PubMed: 29443664]

49. Chan KY et al. Engineered AAVs for efficient noninvasive gene delivery to the central and peripheral nervous systems. Nature neuroscience, doi:10.1038/nn.4593 (2017).

50. Hordeaux J et al. The Neurotropic Properties of AAV-PHP.B Are Limited to C57BL/6J Mice. Molecular therapy : the journal of the American Society of Gene Therapy, doi:10.1016/j.ymthe. 2018.01.018 (2018).

51. Huang Q et al. Delivering genes across the blood-brain barrier: LY6A, a novel cellular receptor for AAV-PHP.B capsids. bioRxiv, 538421, doi:10.1101/538421 (2019).

52. Harvey RJ & Napper RM Quantitative study of granule and Purkinje cells in the cerebellar cortex of the rat. J Comp Neurol 274, 151–157, doi:10.1002/cne.902740202 (1988). [PubMed: 3209738]

53. Vogel MW, Sunter K & Herrup K Numerical matching between granule and Purkinje cells in lurcher chimeric mice: a hypothesis for the trophic rescue of granule cells from target-related cell death. The Journal of neuroscience : the official journal of the Society for Neuroscience 9, 3454–3462 (1989). [PubMed: 2795133]

54. Kim JY et al. Viral transduction of the neonatal brain delivers controllable genetic mosaicism for visualising and manipulating neuronal circuits in vivo. Eur J Neurosci 37, 1203–1220, doi: 10.1111/ejn.12126 (2013). [PubMed: 23347239]

55. Kim JY, Grunke SD, Levites Y, Golde TE & Jankowsky JL Intracerebroventricular viral injection of the neonatal mouse brain for persistent and widespread neuronal transduction. Journal of visualized experiments : JoVE, 51863, doi:10.3791/51863 (2014).

56. Hoxha E, Balbo I, Miniaci MC & Tempia F Purkinje Cell Signaling Deficits in Animal Models of Ataxia. Front Synaptic Neurosci 10, 6, doi:10.3389/fnsyn.2018.00006 (2018). [PubMed: 29760657]

57. Matilla-Duenas A et al. Consensus paper: pathological mechanisms underlying neurodegeneration in spinocerebellar ataxias. Cerebellum 13, 269–302, doi:10.1007/s12311-013-0539-y (2014). [PubMed: 24307138]

58. Chakrabarty P et al. Capsid serotype and timing of injection determines AAV transduction in the neonatal mice brain. PloS one 8, e67680, doi:10.1371/journal.pone.0067680 (2013). [PubMed: 23825679]

59. Madisen L et al. A robust and high-throughput Cre reporting and characterization system for the whole mouse brain. Nature neuroscience 13, 133–140, doi:10.1038/nn.2467 (2010). [PubMed: 20023653]

60. Zinn E et al. In Silico Reconstruction of the Viral Evolutionary Lineage Yields a Potent Gene Therapy Vector. Cell Rep 12, 1056–1068, doi:10.1016/j.celrep.2015.07.019 (2015). [PubMed: 26235624]

61. Koch SF et al. Genetic rescue models refute nonautonomous rod cell death in retinitis pigmentosa. Proc Natl Acad Sci U S A 114, 5259–5264, doi:10.1073/pnas.1615394114 (2017). [PubMed: 28468800]

62. Maeder ML et al. Development of a gene-editing approach to restore vision loss in Leber congenital amaurosis type 10. Nature medicine, doi:10.1038/s41591-018-0327-9 (2019).

63. Park WD et al. Identification of 58 novel mutations in Niemann-Pick disease type C: correlation with biochemical phenotype and importance of PTC1-like domains in NPC1. Hum Mutat 22, 313–325, doi:10.1002/humu.10255 (2003). [PubMed: 12955717]

64. Praggastis M et al. A murine Niemann-Pick C1 I1061T knock-in model recapitulates the pathological features of the most prevalent human disease allele. The Journal of neuroscience : the official journal of the Society for Neuroscience 35, 8091–8106, doi:10.1523/JNEUROSCI. 4173-14.2015 (2015). [PubMed: 26019327]

65. Yu T, Shakkottai VG, Chung C & Lieberman AP Temporal and cell-specific deletion establishes that neuronal Npc1 deficiency is sufficient to mediate neurodegeneration. Human Molecular Genetics 20, 4440–4451, doi:10.1093/hmg/ddr372 (2011). [PubMed: 21856732]

66. Loftus SK et al. Rescue of neurodegeneration in Niemann-Pick C mice by a prion-promoter-driven Npc1 cDNA transgene. Hum Mol Genet 11, 3107–3114 (2002). [PubMed: 12417532]

67. Lopez ME, Klein AD, Dimbil UJ & Scott MP Anatomically defined neuron-based rescue of neurodegenerative Niemann-Pick type C disorder. The Journal of neuroscience : the official journal of the Society for Neuroscience 31, 4367–4378, doi:10.1523/JNEUROSCI.5981-10.2011 (2011). [PubMed: 21430138]

68. Elrick MJ et al. Conditional Niemann-Pick C mice demonstrate cell autonomous Purkinje cell neurodegeneration. Human Molecular Genetics 19, 837–847, doi:10.1093/hmg/ddp552 (2010). [PubMed: 20007718]

69. Ko DC et al. Cell-autonomous death of cerebellar purkinje neurons with autophagy in Niemann-Pick type C disease. PLoS Genet 1, 81–95, doi:10.1371/journal.pgen.0010007 (2005). [PubMed: 16103921]

70. Langmade SJ et al. Pregnane X receptor (PXR) activation: a mechanism for neuroprotection in a mouse model of Niemann-Pick C disease. Proc Natl Acad Sci U S A 103, 13807–13812, doi: 10.1073/pnas.0606218103 (2006). [PubMed: 16940355]

71. Hughes MP et al. AAV9 intracerebroventricular gene therapy improves lifespan, locomotor function and pathology in a mouse model of Niemann-Pick type C1 disease. Hum Mol Genet 27, 3079–3098, doi:10.1093/hmg/ddy212 (2018). [PubMed: 29878115]

72. Ling C et al. High-Efficiency Transduction of Primary Human Hematopoietic Stem/Progenitor Cells by AAV6 Vectors: Strategies for Overcoming Donor-Variation and Implications in Genome Editing. Scientific reports 6, 35495, doi:10.1038/srep35495 (2016). [PubMed: 27759036]

73. Nathwani AC et al. Long-term safety and efficacy of factor IX gene therapy in hemophilia B. N Engl J Med 371, 1994–2004, doi:10.1056/NEJMoa1407309 (2014). [PubMed: 25409372]

74. Chandler RJ et al. Systemic AAV9 gene therapy improves the lifespan of mice with Niemann-Pick disease, type C1. Hum Mol Genet 26, 52–64, doi:10.1093/hmg/ddw367 (2017). [PubMed: 27798114]

75. Xie C, Gong XM, Luo J, Li BL & Song BL AAV9-NPC1 significantly ameliorates Purkinje cell death and behavioral abnormalities in mouse NPC disease. Journal of lipid research 58, 512–518, doi:10.1194/jlr.M071274 (2017). [PubMed: 28053186]

76. Hinderer C et al. Severe Toxicity in Nonhuman Primates and Piglets Following High-Dose Intravenous Administration of an Adeno-Associated Virus Vector Expressing Human SMN. Hum Gene Ther, doi:10.1089/hum.2018.015 (2018).

77. Manno CS et al. Successful transduction of liver in hemophilia by AAV-Factor IX and limitations imposed by the host immune response. Nature medicine 12, 342–347, doi:10.1038/nm1358 (2006).

78. Habib N et al. Massively parallel single-nucleus RNA-seq with DroNc-seq. Nature methods 14, 955–958, doi:10.1038/nmeth.4407 (2017). [PubMed: 28846088]

79. Li P et al. Allele-Specific CRISPR-Cas9 Genome Editing of the Single-Base P23H Mutation for Rhodopsin-Associated Dominant Retinitis Pigmentosa. The CRISPR Journal 1, 55–64, doi: 10.1089/crispr.2017.0009 (2018). [PubMed: 31021187]

80. Sommer C, Strähle C, Köthe U & Hamprecht FA in Eighth IEEE International Symposium on Biomedical Imaging (ISBI 2011). 230–233.

81. Carpenter AE et al. CellProfiler: image analysis software for identifying and quantifying cell phenotypes. Genome Biol 7, R100, doi:10.1186/gb-2006-7-10-r100 (2006). [PubMed: 17076895]

82. Tsai SQ et al. CIRCLE-seq: a highly sensitive in vitro screen for genome-wide CRISPR-Cas9 nuclease off-targets. Nature methods 14, 607–614, doi:10.1038/nmeth.4278 (2017). [PubMed: 28459458]

83. Haeussler M et al. Evaluation of off-target and on-target scoring algorithms and integration into the guide RNA selection tool CRISPOR. Genome Biol 17, 148, doi:10.1186/s13059-016-1012-2 (2016). [PubMed: 27380939]

84. Ullman-Cullere MH & Foltz CJ Body condition scoring: a rapid and accurate method for assessing health status in mice. Lab Anim Sci 49, 319–323 (1999). [PubMed: 10403450]

85. Foltz C & Ullman-Cullere M Guidelines for Assessing the Health and Condition of Mice. Lab Animal 28 (1998).
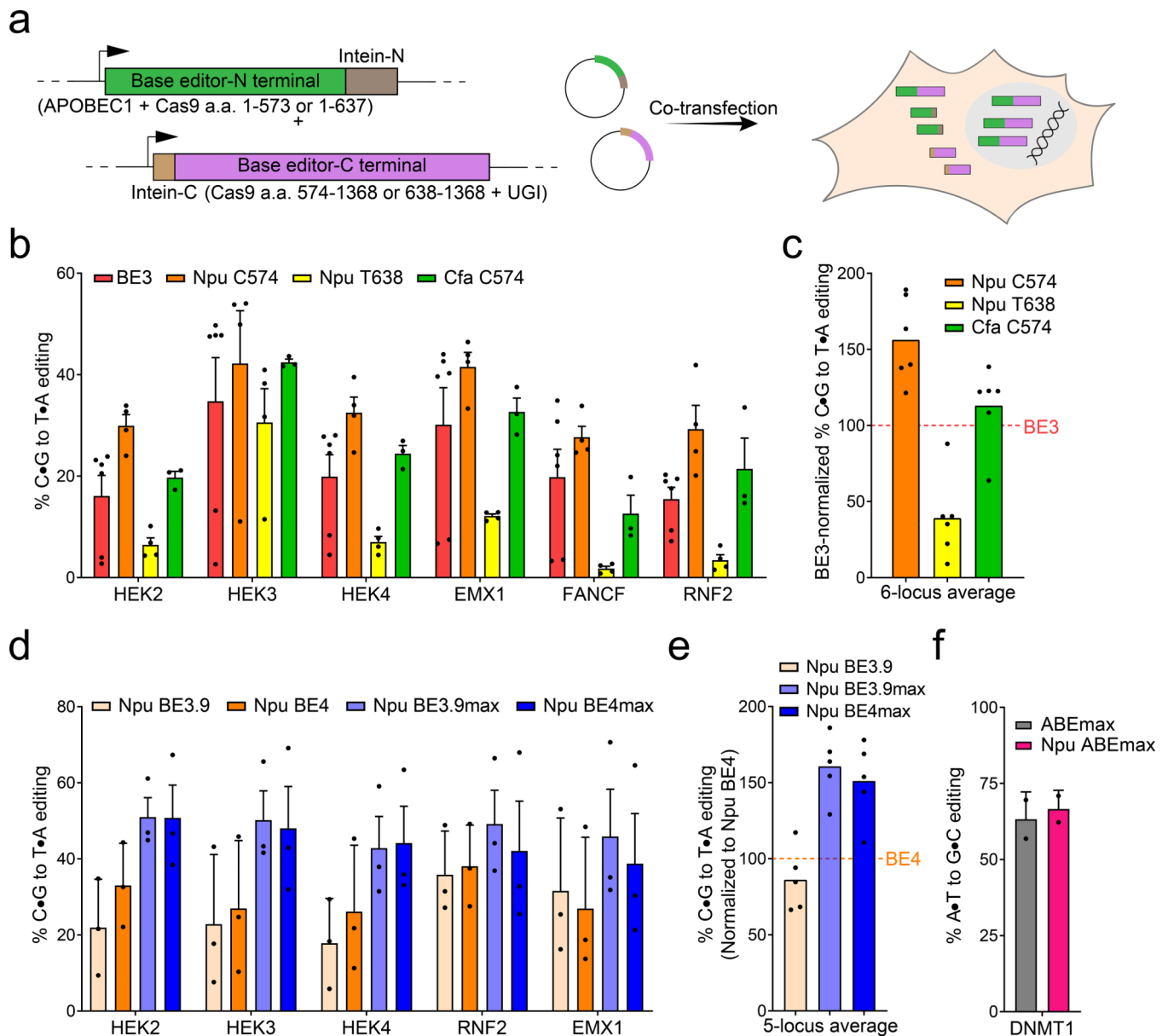
Fig. 1 |. Development of split-intein cytosine and adenine base editors.

a, Intein reconstitution strategy. Two separately encoded protein fragments fused to split-intein halves splice to reconstitute full-length protein following co-expression. **b,** Lipofection of intact BE3 (red), split BE3 with the Npu split-intein site between E573/C574 (orange) or K637/T638 (yellow), or split BE3 with the Cfa split-intein site between E573/C574 (green) into HEK293T cells followed by high-throughput sequencing of six test loci to determine base editing efficiency. **c,** Comparison of average editing data in **(b)**, normalized to BE3 levels (dotted line). BE3-normalized editing at each locus (black dots) was averaged. **d,** "BEmax" optimization of nuclear localization signals and codon usage increases editing efficiency at six standard loci. BE3.9max and BE4max show comparable editing efficiencies. **e,** Comparison of average editing data in **(d)**, normalized to BE4 levels (dotted line). **f,** Lipofection of ABEmax (grey) or Npu-split E573/C574 ABEmax (magenta) into

NIH 3T3 cells for generation of a split-intein adenosine base editor. In **(b)**, **(d)**, and **(f)**, dots represent values and bars represent mean+SD of n=3 **(b)** and **(d)** or n=2 **(f)** independent biological replicates (see Methods for details). Dots in **(c)** and **(e)** represent locus averages.
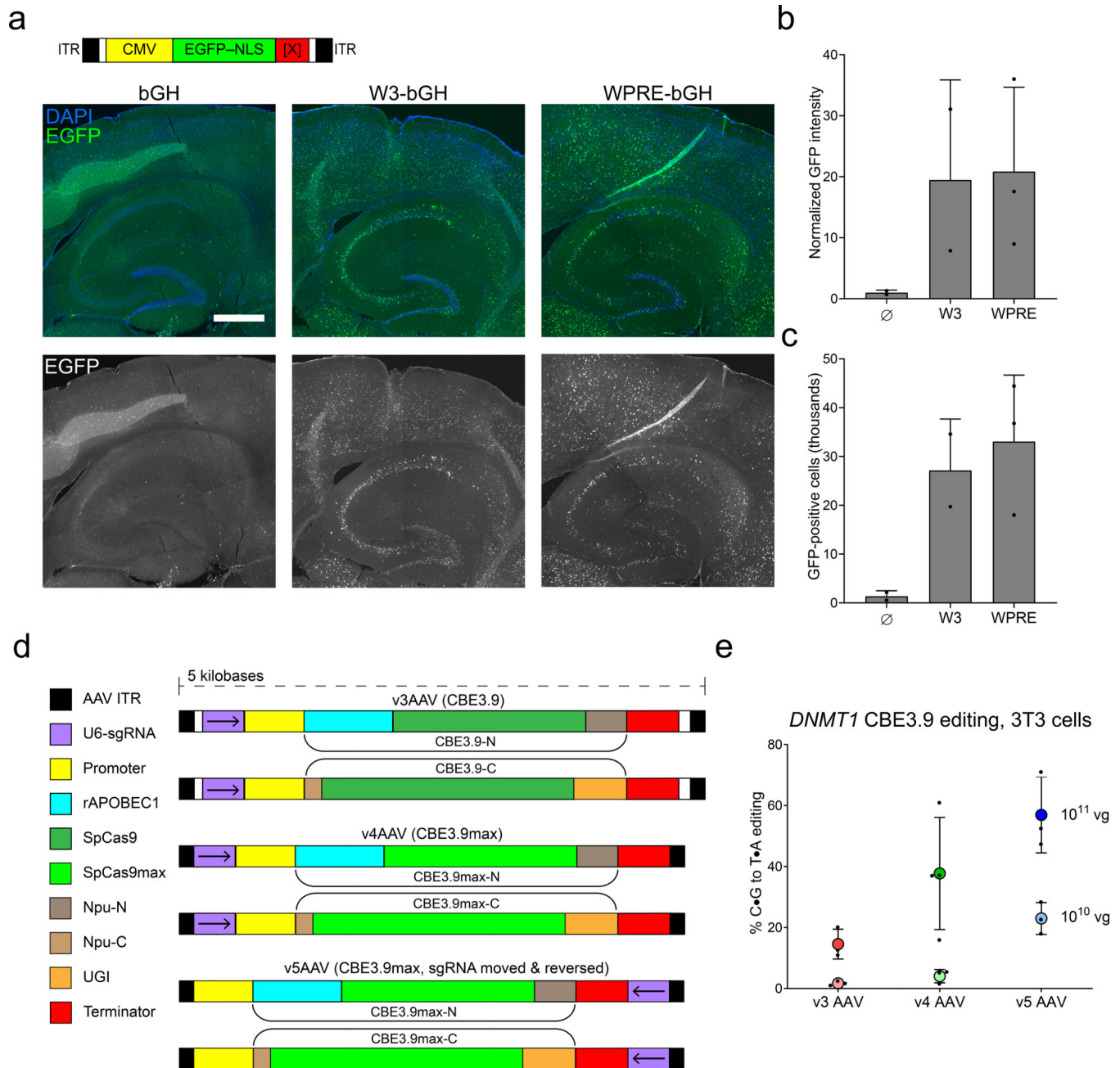
Fig. 2 |. Optimization of split-intein base editor AAVs.
a, GFP expression three weeks after injection of 1×10^{11} vg of GFP–NLS-bGH (n=2 mice, 12 images), GFP–NLS-W3-bGH (n=3 mice, 18 images), or GFP–NLS-WPRE-bGH (n=2 mice, 18 images) into six-week-old C57BL/6 mice. Representative images of horizontal brain slices show hippocampus and neocortex. Top panels show DAPI and EGFP signals overlaid; bottom panels show EGFP signal only. The scale bar represents 500 μm. **b,** Transcriptional regulatory element optimization. Total GFP signal measured by ImageJ from mice described in **(a)**. See methods for a detailed description of imaging and analysis procedures. **c,** Number of GFP-positive cells per horizontal brain slice from the mice

described in **(a)**. GFP-positive cells were identified by ilastik / CellProfiler as described in the image analysis section of the Methods. **d**, Schematic of v3, v4, and v5 AAV variants. Arrows indicate direction of U6 promoter transcription. The CBE3.9 coding sequence consists of rAPOBEC1 (teal), spCas9 D10A nickase (green), and UGI (tan). Small white boxes in v3 are non-essential backbone sequences removed in v4 and v5 AAV. See Supplementary Fig. 2 for the schematic of v5 AAV-ABEmax. **e**, Cytosine base editing efficiencies in NIH 3T3 cells seeded at 50,000 cells/well following a 14-day incubation with the indicated doses of v3 AAV, v4 AAV, and v5 AAV. Dots and bars in **(b)** and **(c)** represent individual replicates and mean+SD of n=2 (bGH and W3-bGH) or n=3 mice (WPRE). Colored circles and error bars in **(e)** represent mean±SD. Dots in **(e)** represent values for independent biological replicates (n=3–4).
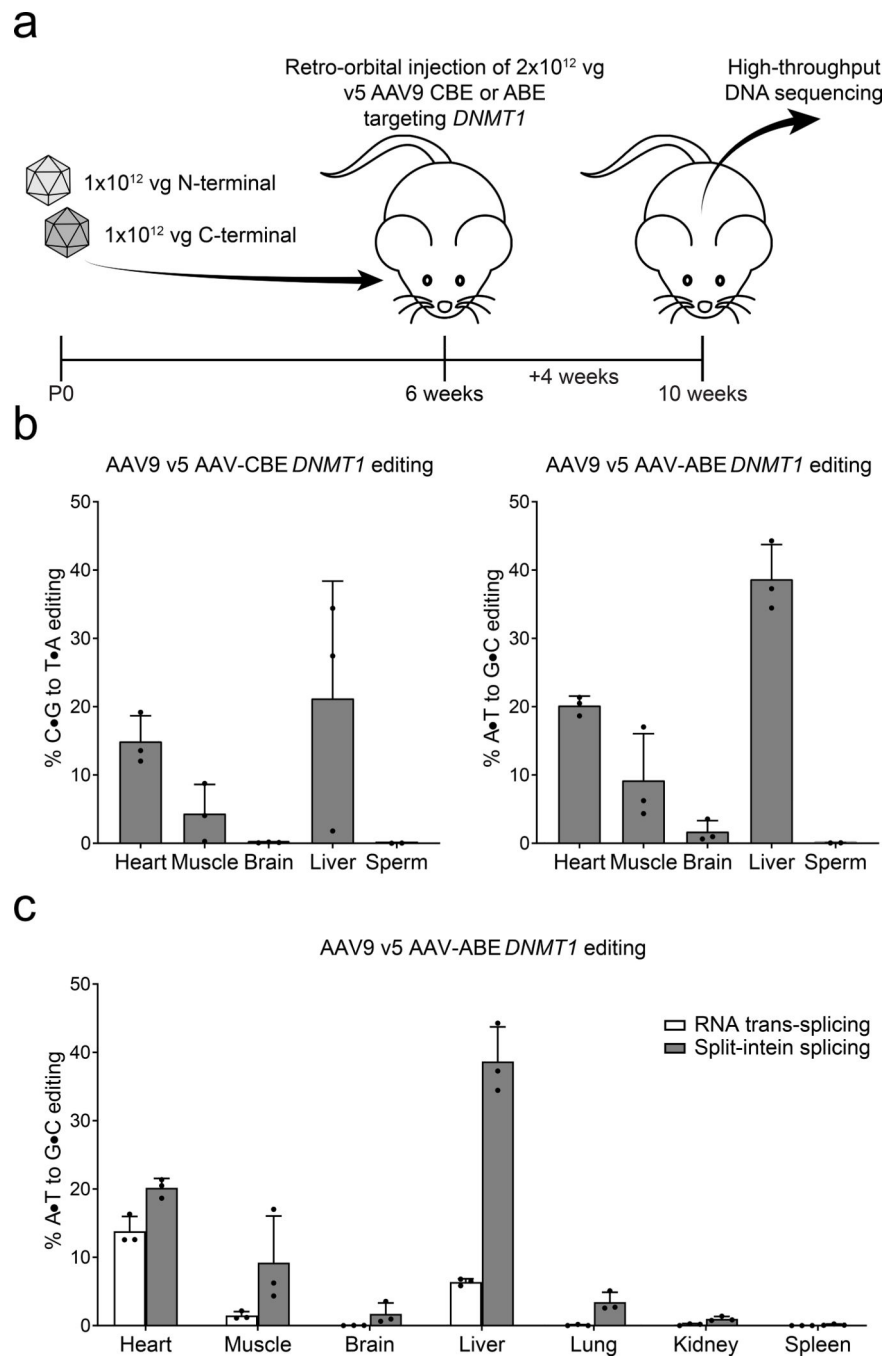
Fig. 3 |. Systemic injection of v5 AAV9 editors results in cytosine and adenine base editing in heart, muscle, and liver.

a, Six-week-old C57BL/6 mice were treated by retro-orbital injection of 2×10^{12} vg total of v5 AAV9. After 4 weeks, organs were harvested and genomic DNA of unsorted cells was sequenced. **b**, Cytosine or adenine base editing by v5 AAV CBE3.9max or v5 AAV ABEmax, respectively, in the indicated organs. **c**, Comparison of adenine base editing from v5 AAV-mediated ABEmax (grey bars) and from trans-mRNA splicing (white bars). The trans-splicing constructs were modified to enable direct comparison by replacing the
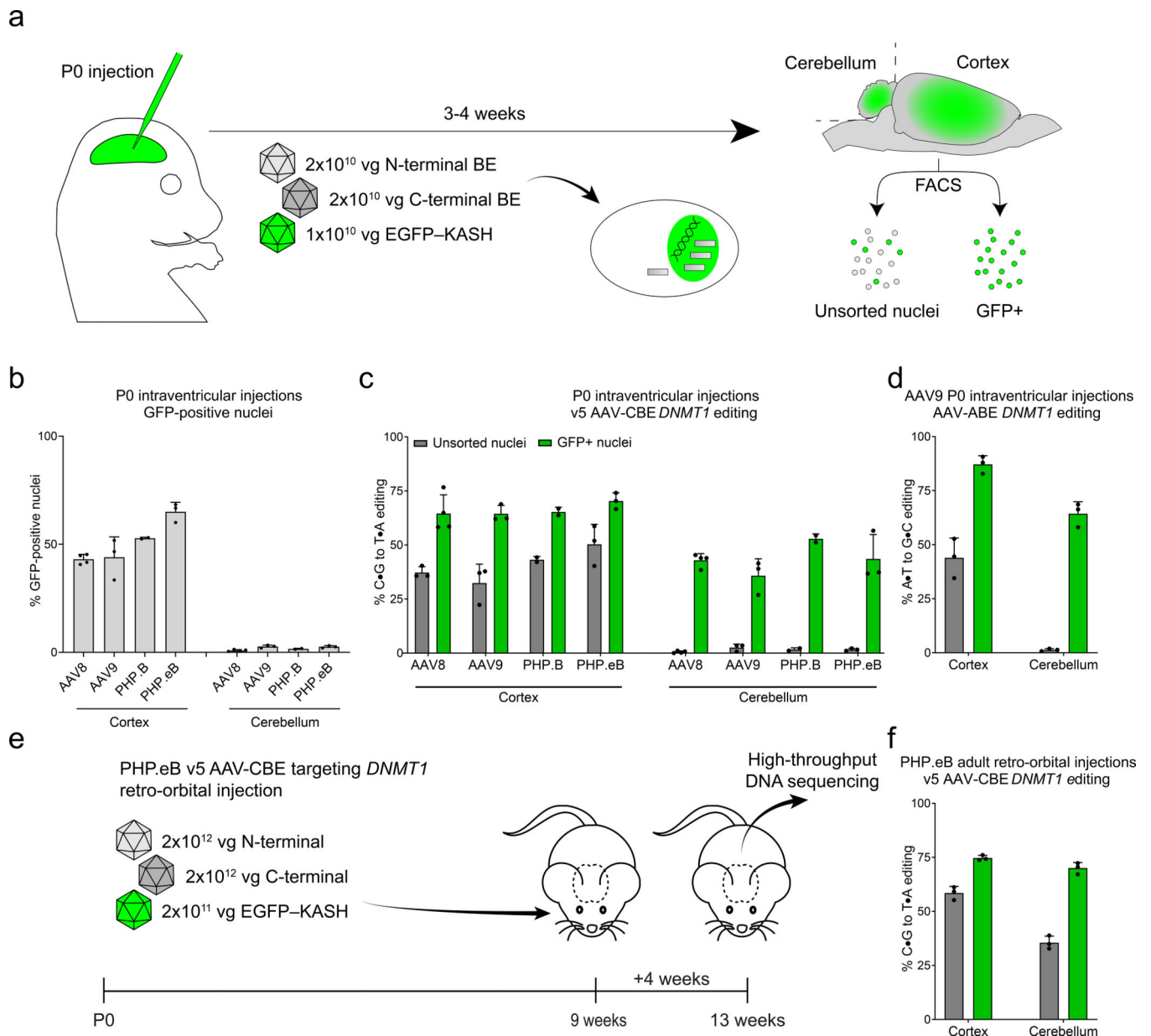
muscle-specific Spc5–12 promoter with the Cbh promoter for ubiquitous expression, and replacing the *DMD*-targeting sgRNA with the *DNMT1*-targeting sgRNA. Bars represent mean+SD of n=3 mice.
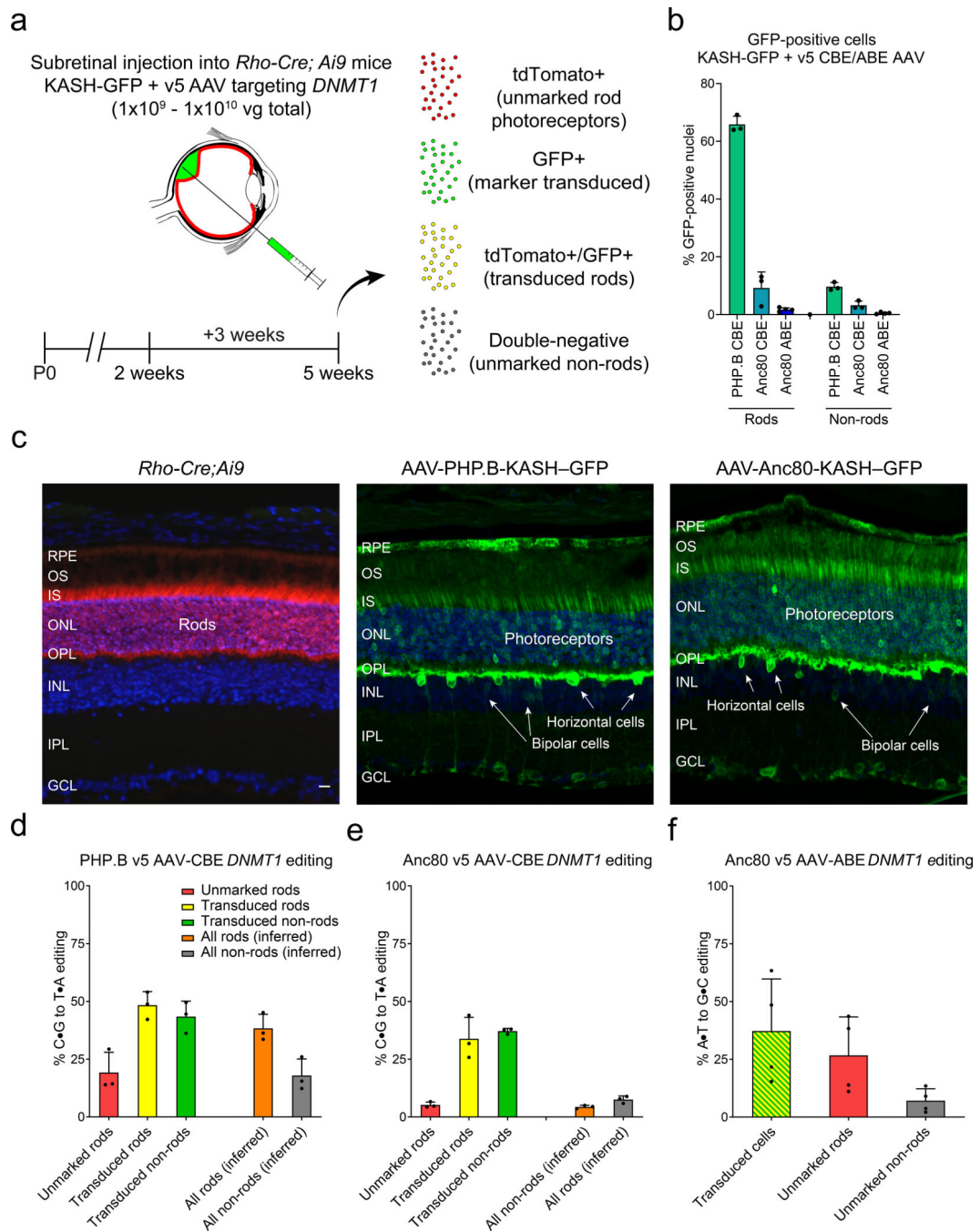
Fig. 4 |. AAV-mediated cytosine and adenine base editing in the central nervous system by two delivery routes.

a, Schematic of P0 intraventricular injections. P0 C57BL/6 mice were co-injected with 4×10^{10} vg total of v5 CBE3.9max or ABEmax AAV targeting *DNMT1* and 1×10^{10} vg Cbh-KASH–GFP. Sorting for GFP-positive cells enriches for triply transduced cells. Tissue was harvested 3–4 weeks after injection, and cortex and cerebellum were separated. Cortical tissue comprises neocortex and hippocampus. For each tissue, nuclei were dissociated and analyzed as unsorted (all nuclei) or GFP-positive populations for DNA sequencing. **b**, Percent GFP-positive nuclei measured by flow cytometry following P0 injection. **c**, Cytosine base editing efficiency following P0 v5 CBE3.9max AAV injection in cortex and cerebellum at *DNMT1* for unsorted nuclei (grey) and GFP-positive nuclei (green) (For **(b)** and **(c)**, AAV8, n=4; AAV9, n=3; PHPB, n=2; PHPeB; n=3). **d**, Adenosine base editing efficiency

following P0 v5 CBE3.9max AAV9 injection in cortex and cerebellum at *DNMT1* for unsorted nuclei (grey) and GFP-positive nuclei (green) (n=3). **e**, Schematic of retro-orbital injections. Brains from 9-week-old C57BL/6 mice were harvested 4 weeks after injection with 4×10^{12} vg total v5 CBE3.9max or ABEmax AAV targeting *DNMT1* and 2×10^{11} vg KASH–GFP AAV, then processed and analyzed as described in Fig. 4. **f**, Cytosine base editing in unsorted (grey) and GFP-positive (green) cortical and cerebellar cells following the procedure described in **(a)** (n=3). In all cases, bars represent mean+SD. Black dots represent individual mice.

Fig. 5 |. AAV-mediated cytosine and adenine base editing in the retina following sub-retinal injections of 2-week-old _Rho-Cre;Ai9_ mice.

a, Schematic of sub-retinal injections. Two-week-old _Rho-Cre; Ai9_ mice were treated by sub-retinal injection of 1×10^9 to 1×10^{10} vg total of v5 CBE3.9max or v5 ABEmax AAV targeting _DNMT1_. Three weeks after injection, injected retinas were sorted into GFP-negative/tdTomato-positive (rod photoreceptors not transduced with GFP; red bars), tdTomato-positive/GFP-positive (transduced rods; yellow bars), GFP-positive/tdTomato-negative (marker transduced non-rods; green bars), and double-negative populations

(unmarked non-rods, not shown). **b**, Percentage of GFP transduced rod photoreceptors or non-rod retinal cells followed by subretinal injection of AAV mix of PHP.B-CBE, Anc80-CBE and Anc80-ABE AAV, respectively. The dose of AAV-GFP is 2×10^9 vg for PHP.B-CBE mix, 3.3×10^8 vg for Anc80-CBE mix and 4.5×10^8 vg for Anc80-ABE mix. **c**, Expression of tdTomato in the rod photoreceptor cells of Rho-Cre;Ai9 mice (left panel). Retinal transduction of PHP.B-GFP (middle panel) or Anc80-GFP (right panel) at 5×10^9 vg. Scale bar = 20 μm. The images are representative of n=2 independent experiments. **d**, Cytosine base editing by v5 CBE3.9max PHP.B AAV in injected retinas. Retinas were injected with 6.5×10^8 vg of each split-editor half. Editing percentage in all rods (orange bars) was inferred as ((editing % in GFP transduced rods)*(number of transduced rods) + (editing % in unmarked rods)*(number of unmarked rods)) / total rods. This calculation was repeated for non-rods (grey bars). **e**, Cytosine base editing by v5 CBE3.9max Anc80 AAV in photoreceptors and other retinal cells. Retinas were injected with 4×10^9 vg of each split-editor half. Editing efficiencies in all rods (orange bars) and all non-rods (grey bars) were inferred as described for **(b)**. **f,** Adenine base editing by v5 ABEmax Anc80 AAV in photoreceptors. Retinas were injected with 4.5×10^8 vg of each split-editor half. All GFP-positive cells were pooled in this experiment, resulting in a single GFP-positive population containing tdTomato-positive and tdTomato-negative cells (yellow/green bar).. Black dots represent individual eyes. For **(b)** and **(d)** - **(f)**, bars represent mean+SD of independent injections (PHP.B-CBE, n=3; Anc80-CBE, n=3; Anc80-ABE, n=4).
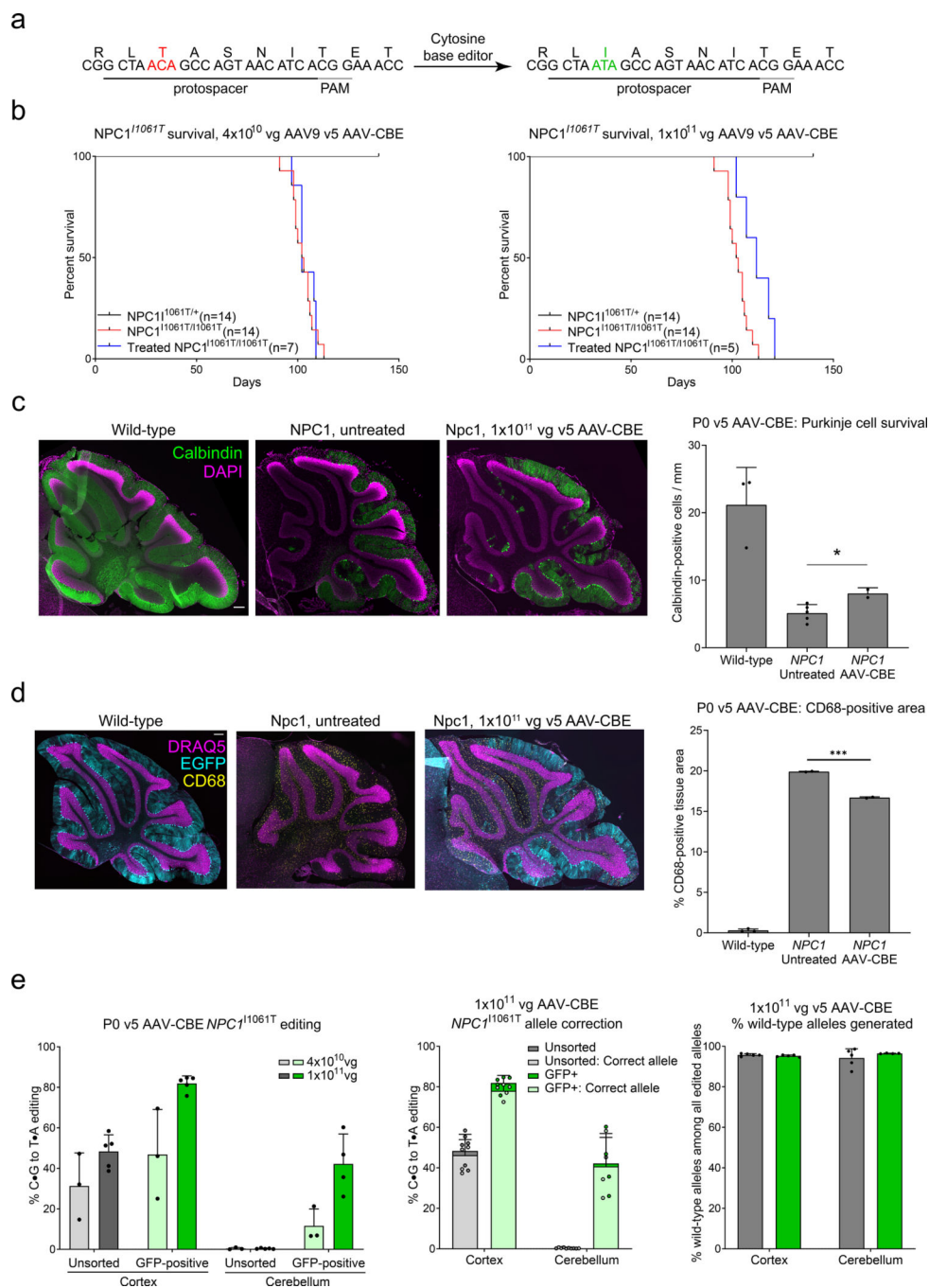
Fig. 6 |. Base editing of $Npc1^{I1061T}$ in the mouse CNS.

a, Schematic of the $Npc1$ locus highlighting the mutation in exon 21, the protospacer and PAM sequence targeted, and the desired CBE-mediated reversion of I1061T. The scale bar represents 5 kilobases. **b**, Kaplan-Meier plots of untreated homozygous $Npc1^{I1061T}$ mice (red; n=14), $Npc1^{I1061T}$ heterozygous mice (black; n=14), and mice injected with either 4×10^{10} vg total of v5 CBE3.9max AAV9 targeting $NPC1^{I1061T}$ (left plot, blue; n=7), or with 1×10^{11} vg total v5 CBE3.9max AAV9 targeting $Npc1^{I1061T}$ (right plot, blue; n=5). Following 1×10^{11} vg injection, the median survival increases from 102.5 to 112 days,

p=0.02 by Mantel-Cox test. **c**, Immunofluorescent measurement of Purkinje cell survival. Images are representative Calbindin-stained midline sagittal cerebellar slices from P98-P105 mice. Surviving calbindin-positive cells appear in green, and DAPI is pseudocolored magenta. In the quantification of imaging data, each point represents the average number of Purkinje cells per slice for each mouse. Wild-type, n=3 mice, 9 images; $Npc1^{I1061T}$ untreated, n=5 mice, 20 images; $Npc1^{I1061T}$ AAV-CBE, n=2 mice, 16 images. Untreated vs. treated, two-sided t-test, p= 0.0327. **d**, Immunofluorescent measurement of CD68$^+$ tissue area. Images are representative CD68-stained midline saggital cerebellar slices from P98-P105 mice. EGFP–KASH labeled cells appear in cyan, CD68$^+$ cells appear in yellow, and DRAQ5 signal is pseudocolored magenta. The untreated mice are uninjected and do not express GFP. In the quantification of CD68$^+$ tissue area, each point represents the average per mouse. Wild-type, n=3 mice, 15 images; $Npc1^{I1061T}$ untreated, n=2 mice, 6 images; $Npc1^{I1061T}$ AAV-CBE, n=2 mice, 10 images. Untreated vs. treated, two-sided t-test, p=0.0005. **e**, Cortical and cerebellar base editing in P0 mice injected with v5 AAV9 targeting $Npc1^{I1061T}$. In the left subpanel, lighter bars report editing in unsorted (grey) or GFP-positive (green) cells following injection of n=3 mice with 4×10^{10} vg (2×10^{10} vg of each split base editor half); darker bars correspond to editing following injection of n=5 mice with 1×10^{11} vg (5×10^{10} vg of each split base editor half). The middle subpanel reports base editing to the precisely corrected wild-type allele shown in **(a)** from the 1×10^{11} vg injections. Lighter bars indicate the frequency of alleles that are corrected to the wild-type sequence; replotted darker bars indicate total C•G-to-T•A editing of the T1061 codon colored red in **(a)**. The right subpanel shows precisely corrected (wild-type) alleles as a percentage of all edited alleles in mice injected with 1×10^{11} vg. In **(b)**, tick marks indicate animal deaths. In all other panels, bars represent mean+SD. Dots represent individual mice. Scale bars represent 200 μm. Statistical tests for immunofluorescence are two-sided t-tests without multiple comparison corrections.